IEEE Access
Multidisciplinary | Rapid Review | Open Access Journal

Received March 4, 2022, accepted March 28, 2022, date of publication March 31, 2022, date of current version April 13, 2022.

Digital Object Identifier 10.1109/ACCESS.2022.3163708

Comparison and Influence of Flywheels Energy Storage System Control Schemes in the Frequency Regulation of Isolated Power Systems

HILEL GARCÍA-PEREIRA[1], MARCOS BLANCO[2], GUILLERMO MARTÍNEZ-LUCAS[1], JUAN I. PÉREZ-DÍAZ[1], AND JOSÉ-IGNACIO SARASÚA[1]

[1]Department of Hydraulic, Energy and Environmental Engineering, Universidad Politécnica de Madrid, 28040 Madrid, Spain
[2]CIEMAT, Spanish National Research Centre on Energy, Environment and Technology, 28040 Madrid, Spain

Corresponding author: José-Ignacio Sarasúa (joseignacio.sarasua@upm.es)

This work was supported by the Regional Ministry of Science, University and Innovation of Community of Madrid, through the Project 'Sizing and Control of Flywheel Energy Storage Power Plants in Isolated Power Systems with High Renewable Penetration' of the Multiannual Agreement Between Community of Madrid and the Universidad Politécnica de Madrid, under Grant APOYO-JOVENES-SU3JLM-61-6XFZ49.

ABSTRACT Increased renewable energy penetration in isolated power systems has a clear impact on the quality of system frequency. The flywheel energy storage system (FESS) is a mature technology with a fast frequency response, high power density, high round-trip efficiency, low maintenance, no depth of discharge effects, and resilience to withstand continuous charge-discharge cycling without lifetime degradation. These FESS properties allows to effectively address the frequency quality problem. This study analyzes the contribution of a FESS to reducing frequency deviations in an isolated system that combines a diesel plant, wind farm, and pump-storage hydropower plant based on the El Hierro power system. This study approaches this analysis by comparing six different FESS governor control schemes (GCSs). Of these six GCSs, the nonlinear proportional variant (NLP_V) is a singular contribution based on the NLP scheme previously developed by the same researchers. Different governor's parameter settings for the FESS GCSs were also compared, obtained from the proposed tuning methodology that considers the renewable energy generation distribution, frequency impact, and lifetime degradation of diesel, hydraulic groups, and flywheels. The GCSs were compared in terms of average frequency deviation, Zenith and Nadir frequency difference, wear and tear of diesel electromechanical elements and Pelton turbine nozzles, flywheels cycles per hour, and FESS average state of charge. The results show that including a FESS plant considerably improves frequency regulation. The tuning criteria and GCSs have a clear influence on the results, with NLP and NLP_V GCSs offering relevant improvements in frequency deviations.

INDEX TERMS Flywheel control scheme, flywheel energy storage, frequency control, hybrid power systems, isolated system, power system stability.

NOMENCLATURE AND ABBREVIATIONS

f	Frequency (p.u.).
D	Damping (p.u.).
p_d	Load demand power (p.u.).
p_{DG}	Power delivered by diesel groups (p.u.).
p_{FESS}	Power supplied or absorbed by flywheels (p.u.).
p_H	Power delivered by Pelton turbines (p.u.).
p_p	Power absorbed by pumps (p.u.).
p_w	Power delivered by the wind turbines (p.u.).
R	Droop (Hz/MW).
T_m	Mechanical starting time (s).
T_{FESS}	time constant of the first order transfer function of the FESS – grid connection (s).
AGC	Automatic generation control.
AVFD	Average frequency deviation (Hz).
DB	Droop based.
DB_V	Droop based variant.
DPP	Diesel power plant.
FESS	Flywheel energy storage system.

The associate editor coordinating the review of this manuscript and approving it for publication was Behnam Mohammadi-Ivatloo.

GCSs	Governor control schemes.
NLP	Nonlinear proportional.
NLP_V	Nonlinear proportional variant.
PD	Proportional derivative.
PD_V	Proportional derivative variant.
PSHP	Pumped storage hydropower plant.
Q1	Frequency quality objective.
Q2	Aggregated remaining lifetime of diesel units, Pelton turbines and flywheels objective.
RE	Renewable energy.
RoCoF	Rate of change of frequency.
SOC	State of charge (p.u.).
VSWT	Variable speed wind turbine.
WaT	Wear and tear of diesel electromechanical elements and Pelton turbines nozzles (p.u./s).

I. INTRODUCTION

Increasing renewable energy (RE) penetration in power systems is a challenge that has been constantly addressed in recent decades [1] to reduce greenhouse gas emissions from traditional energy systems. According to the agreement reached by the European Council [2] in October 2014, at least 27% of the final energy consumption should be covered by RE in 2030. This percentage should increase to at least two-thirds by 2050, according to the European energy roadmap [3].

Increasing RE penetration in isolated power systems is particularly interesting because reducing the use of fossil fuels has an obvious environmental benefit [4]. Furthermore, since traditional energy generation costs in isolated power systems are expensive, RE generation can offer some crucial economic advantages, such as reducing important transport costs and energy dependency, which are typical characteristics of these systems, and islands in particular [5]–[7].

Variable RE penetration in power systems has some inherent drawbacks such as unmanageability [8] and resource variability [9], [10]. Specifically, the variability in the medium (in a range of minutes) and short term (in a range of seconds) has a negative impact on the system reliability, causing a deterioration of the system frequency quality both in interconnected [11], [12] and isolated systems [10], [13]. Another negative impact of RE generation is the reduction of the system synchronous inertia, because in many cases RE is connected to the power systems through power electronic converters [8]. Therefore, small isolated power systems, which are inherently weak in terms of inertia, are most affected by the increased RE penetration and power imbalances. For example, the intermittency of wind generation in Hawaii, according to Kaneshiro [10], can reduce wind farm power at a ratio of 1 MW/min, severely affecting system security and stability, to the point that the power system operator developed a specific action plan to dispatch selected units to compensate for wind variation.

To ensure that the isolated power system can operate safely in high RE penetration scenarios, load shedding is a regular but undesirable practice to avoid frequency deviations [14]. One drastic measure to avoid this practice is limiting the generation of RE, usually referenced as curtailment (defined as a reduction in the output of RE generator from what it could otherwise produce given available RE resources), such as in Portuguese island of Flores, where wind energy penetration is limited [15], French islands of Martinique and Réunion, where a policy limits maximum RE penetration to 30% [16], or Scottish islands of Orkney, where different wind-energy curtailment schemes are deployed to increase the power system controllability [17].

Technical solutions to improve the integration of RE in isolated systems and to avoid frequency deviations have been extensively researched. The most popular methods found in the related literature include (i) implementation of synthetic inertia and frequency control support, a very extended method in very different RE scenarios such as solar-thermal hybrid systems [18], tidal generation [19], variable-speed wind turbines and power converters [20]–[25], and even with electric vehicles connected to the grid to provide grid support services [26], [27], (ii) development of better prediction models to reduce variable RE uncertainty [28], [29], (iii) addition of real inertia by synchronous condensers [30], (iv) pump storage hydropower plants participating in frequency regulation when pumping [31]–[33] and - probably the most common option - (v) utilization of auxiliary energy storage systems [34], [35] such as batteries, capacitors, superconductors or flywheels to provide fast frequency response and inertial response.

If we focus on the utilization of auxiliary energy storage systems, the most important requirements to participate in frequency regulation (complementing variable RE technologies) are storage capacity, power output, and a sufficiently fast frequency response capability [36], as summarized in the grid codes and policies established by several countries [37].

Among all energy storage systems, FESS is a very interesting technology for frequency regulation due to its maturity, and good technical and exploitation properties. According to [38] flywheels are one of the best energy storage systems as synthetic inertia source compared to fuel cells, supercapacitors and lithium-ion based batteries. The low costs for operation and maintenance and long cycle life of flywheels (typically 20 years) with almost no depth of discharge effects and high round trip efficiency, result in very low effective cost per cycle compared to other storage technologies as stated in [39] where power costs (US$/kW) and energy costs (US$/kWh) of some successful FESS plants offering grid services until year 2015 are summarized. Another advantage of flywheels is their power ramp rate that allows them to provide full power in less than 50-60 ms and change from supplying power to absorbing power in 10 ms [40]. Recent state of art of flywheels conducted in 2022 [41] shows that FESS technology can be used in several different fields, where some of the existing research groups and commercials FESS are

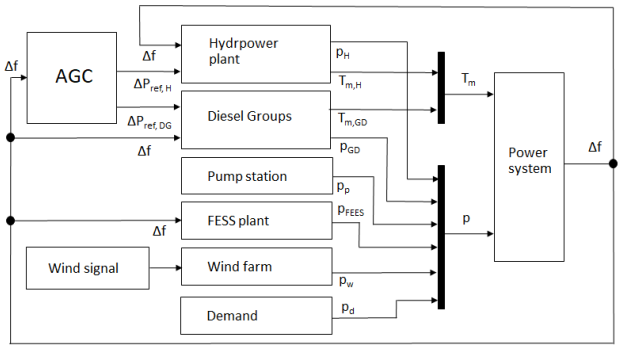

FIGURE 1. Block diagram of the isolated electric system dynamic model.

shown with their characteristics. Some FESS examples of real facilities that operate for frequency regulation purposes in different power systems can be found in [42], [43].

The state of development of flywheels gives them the opportunity to participate in frequency support in high RE penetration scenarios and, consequently, in several new strategies to efficiently operate the power systems.

Different governor control schemes (GCSs) can be found in the literature when the FESS participates in the power system frequency regulation of isolated systems where variable RE is present (usually wind and solar). The classical approach consists of a droop-based (DB) GCS, where the FESS power output is proportional to the frequency deviations [44]. Recent hardware-in-the-loop testing of FESS according to the Germany grid code [45] further validates the application of FESS in frequency support services and that FESS DB governor action is relevant in this service. Sami *et al.* [46] modified classical DB control by introducing a variable deadband function of the state of charge (SOC). Research of control schemes based on synthetic inertia offered by flywheels is still popular nowadays, as in [47] where flywheels are a valuable source of inertial frequency support to prevent an undesired frequency Nadir in a multi-area frequency model. In [38], the viability of energy storage technologies as synthetic inertia sources is discussed and in [40] FESS capability to provide this service is presented. According to Sebastian and Alzola [48] FESS power response is based on a proportional action according to the frequency deviation and synthetic inertia based on rate of change of frequency (RoCoF) by processing the frequency signal with a proportional derivative (PD) controller. Takahashi and Tamura [49] established the FESS power setpoint as a combined function of the system frequency deviation and FESS SOC deviation (computed as the deviation from the 50% SOC level). As in [48], the frequency deviation is processed by a PD controller, whereas the FESS SOC deviation is processed by a proportional controller.

Sarasua *et al.* [50] proposed a different approach with a nonlinear proportional (NLP) GCS, where the FESS power setpoint depends on the SOC level and the distance between the actual SOC and the maximum/minimum SOC.

To the knowledge of the authors, no previous research has identified the differences and drawbacks of previously explained GCSs and compared them. Moreover, the impact of FESS frequency regulation on wear and tear in other existing facilities that participate in frequency regulation or whether the GCS behavior is compatible with the flywheel lifetime offered by manufacturers has not been studied.

Another missing topic in related research is a clear methodology for tuning the governors' parameter settings for a wide operating range of power system configurations. In previously cited studies, GCSs were tested under one specific power system configuration, whereas actual power systems usually have a wide range of operating configurations according to RE generation, which is directly linked to renewable resource availability.

To realistically address all of these issues, the authors' approach is based on a simulation comparison and analysis of a dynamic model with highly variable RE penetration using MATLAB-Simulink. The dynamic model has been elaborated using as a case study the El Hierro Island power system, where frequency deviations are common due to high wind penetration [51]. The model includes a power system, a pumped storage hydropower plant, a variable-speed wind turbine farm, a diesel power plant, and a new FESS plant. The model allows reproducing the evolution of frequency deviations under different scenarios of wind penetration to compare the impact of a FESS plant under different GCSs and governor's parameter settings for each GCS.

In this manner, based on the case study model analysis and the multiple simulations that have been carried out, the main contributions of this study include (i) proposing a new GCS for the FESS based on improving the NLP GCS, (ii) creating a methodology to tune the FESS governor's tunable parameters that considers the RE generation mix scenario, and both the impact on system frequency and wear and tear that diesel and hydraulic groups suffer, and (iii) comparing different GCSs for the FESS under different generation scenarios and governor's parameter settings (obtained from the application of different tuning criteria).

This study is organized as follows. In **Section II**, the dynamic model of the power system developed in MATLAB-Simulink is presented. The proposed FESS GCSs are described in **Section III**. In **Section IV**, the proposed FESS governor tuning methodology is described. In **Section V**, the case study analysis and comparison of results are presented, and in **Section VI**, the main conclusions of this study are outlined.

II. MODEL DESCRIPTION

An aggregated inertial dynamic model that reproduces the frequency deviations of a power system was developed to check the effectiveness of a FESS plant, the viability of different FESS GCSs, and how the system reacts under different governor's parameter settings in different scenarios of wind penetration and power generation.

The model replicates a small islanded isolated power, where RE penetration is high, and frequency deviations are common. Various power-generating technologies are present in this power system: a wind farm, pumped storage hydropower plant (PSHP), and conventional generation by a diesel power plant (DPP).

Power system frequency control is carried out first by inertial response, second by primary regulation based on droop characteristics, and finally by secondary regulation, restoring the system frequency to the reference level. Secondary regulation participating generators are coordinated by automatic generation control (AGC).

The model was implemented in MATLAB-Simulink. The main components of the model are the power system, DPP, wind farm, pumping station, hydropower plant, AGC, and introduced FESS plant. This model is highly configurable and can be adapted to other similar isolated power systems. A model block diagram is presented in FIGURE 1.

All equations used to build each of the different subsystems included in the model (described in the following subsections), and their corresponding nomenclature, are presented in the Appendix.

The proposed system model does not consider power lines because their influence on the grid frequency is negligible owing to the limited power system size.

Wind profiles play an important role in determining the frequency dynamic response of the system, because they are the main source of frequency deviations. The wind profiles are input into the model. To reduce the frequency deviations introduced by wind speed variability, this study focuses on changing the FESS GCS and governor's parameter settings of each GCS, analyzing the output grid frequency evolution, and other study variables to determine their feasibility.

A. POWER SYSTEM

An aggregated inertial model was used to represent the power system. This model successfully reproduces the system frequency deviations when the power system allows generators and loads to be lumped together, which typically occurs when the power system capacity is small, as in islands and isolated power systems. This aggregated inertial model approach was successfully used in the Irish power system [52]. Other examples of inertial model approaches can be found in [53] and [54].

This model is based on the principle that frequency (f) deviations are the result of the imbalance between the sum of power generation (hydroelectric [p_H], diesel groups [p_{DG}], and wind farm [p_w]) and the sum of power consumption (pumping [p_p] and power demand [p_d]), based on equation (1). It is important to note that the FESS can provide ($p_{FESS} > 0$) or absorb ($p_{FESS} < 0$) power according to the system needs.

$$f\frac{df}{dt} = \frac{1}{T_m}(p_H + p_w + p_{DG} \pm p_{FESS} - p_p - p_d - D \cdot \Delta f) \tag{1}$$

Inertial mechanical time (T_m) refers to the inertia offered by traditional synchronous generators directly connected to the grid (in this case PSHP and DPP). D refers to the damping effect and includes the sensitivity of the consumer load to frequency variations.

B. PUMPING STATION

The pumping station is composed of both fixed-speed and variable-speed pumps. A complete model of the conduits and hydraulic machines was used, in addition to a simplified electric machine model, to represent the dynamic response of the pumping station. This model was described in [33].

The hydraulic circuit connecting the lower and upper reservoirs is composed of a penstock, manifold, and several pipes that join the manifold downstream from each pump. To model its dynamic response, a lumped parameter approach that considers both the elastic phenomena of the penstock and water compressibility was used.

To model the pumps, quadratic equations and hydraulic similarity were used to express the relationship between flow, rotational speed, mechanical power, and net head. Because the model objective is frequency regulation in tens of seconds, electric machine models have been simplified and do not consider electric transients using a transfer function equivalent to the asynchronous machine dynamic equation. The imbalance between the electrical and mechanical torques determines the rotational speed deviations.

C. HYDROPOWER PLANT

Similar to the pumping station, a complete model of Pelton turbines and conduits was used in addition to a simplified electric machine model to replicate the dynamic response of the hydropower plant. The characteristics of this model were described in [55].

The hydraulic circuit was modeled in a manner similar to that of the pump station. The upper reservoir and turbines were connected through a long penstock divided in a manifold (at the same point) in several short pipes close to the Pelton turbines downstream. A lumped parameter approach that considers both the elastic phenomena of the penstock and the water compressibility was used.

Pelton turbine models were created considering the relationship between the head, flow, and nozzle opening. Electrical machine models were also simplified and based on a transfer function equivalent to the synchronous machine dynamic equation.

D. DIESEL POWER PLANT

The DPP is composed of diesel groups of different sizes with different power outputs. To represent the dynamic response, a transfer function model was implemented for each generator [56] based on its technical characteristics, obtained from the Llanos Blancos power plant environmental declaration [57].

E. WIND FARM

VSWTs comprise the wind farm. Each VSWT model was extracted from [58] and included the control scheme model for the pitch angle and electromechanical model of the wind turbine generator.

The pitch angle model allows for smooth wind power generation by controlling the wind input torque. The wind turbine generator model includes a rotor inertial expression to compute the rotor speed variances from the imbalance between the mechanical torque and electrical torque demanded by the power converter.

The wind farm model input is the wind speed profile, whereas the output is the electric power generated by the VSWTs.

F. AGC

The AGC model was described in [56] and implemented to coordinate the generators that participate in secondary frequency regulation. This secondary regulation is, an automatic control that triggers when an under-frequency deviation is maintained for more than 30s and primary frequency regulation does not manage to fix the problem. The pump station, hydropower plant Pelton turbines, and DPP provide this service.

G. FESS PLANT

The FESS model was implemented to provide a fast frequency response to mitigate the effect of wind-power fluctuations on the grid frequency. The FESS plant model has two main components: the flywheel governor and flywheel device model. The block diagram is presented in FIGURE 2.

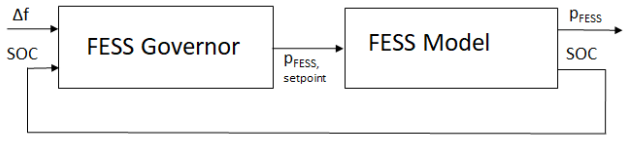

FIGURE 2. Block diagram of the FESS plant.

The FESS plant model includes several identical flywheels and a governor where different control schemes are implemented.

The FESS model also includes a first order transfer function that simulates the connection between the FESS plant and the grid. In this manner, the power dynamics of the FESS power grid converter and transformer have been considered. The time constant T_{FESS} of the first order transfer function has a value of 0.015s. This value has been chosen based on [40], [45].

$$\frac{1}{T_{FESS} \cdot s + 1} \tag{2}$$

The flywheel governor receives the grid frequency as input and provides the power setpoint signal that the flywheel must supply or absorb from the grid as output. In this study, six different governors have been implemented based on different control schemes and they can be divided into two groups depending on whether the governor only uses the grid frequency as input or if it also uses the SOC as input.

Flywheel governors, named after their working principles, are droop based (DB), Droop Based Variant (DB_V), Proportional Derivative (PD), Proportional Derivative Variant (PD_V), Nonlinear Proportional (NLP) and Nonlinear Proportional Variant (NLP_V). Variant governors always include the frequency and SOC as inputs, as explained in Section III.

The flywheel device model receives as input the power setpoint signal provided by the flywheel governor and outputs both the SOC and the power required (which can be either positive if the flywheels supply power, or negative if the flywheels absorb power). The working principle of the model is based on the difference in torque between the mechanical and electric torques, where the electric torque is defined by the power system requirement (FESS governor signal).

The flywheel model is defined by a set of parameters such as flywheel inertia, self-discharge coefficient, rotational speed range, power, energy capacity, and efficiency [59]. In the model developed for this study, the parameters and dependences were obtained from a real laboratory 25 kW prototype with a capacity of 2.77 kWh.

The set of flywheels are assumed to operate simultaneously, and it is assumed that they can provide maximum power (±25 kW in this case) throughout their entire operating range.

III. FESS GOVERNOR CONTROL SCHEMES

As previously mentioned, six different governor control schemes (GCSs) for the FESS plant were implemented and studied. Four of these GCSs are based on a bibliography review: droop based (DB) [44], droop based variant (DB_V) [46], proportional derivative (PD) [48], and proportional derivative variant (PD_V) [49] The nonlinear proportional (NLP) scheme has been previously by the researcher team of the authors [50] and nonlinear proportional variant (NLP_V) is a contribution of this study.

In the first approximation, the GCSs can be divided into two groups: standard GCSs and "variant" GCSs. Every GCS has a power system frequency as the input. "Variant" GCSs singularity is that they always add the SOC of the flywheels as an input in their control loops besides the power system frequency (which is the target variable to control). As output, the FESS governor provides the power setpoint reference that the flywheels should provide or absorb to the grid.

In this study, the sign criterion is as follows: power is positive when the FESS supplies power to the grid in a discharge process and negative when the FESS absorbs power from the grid in a charge process.

In each GCS, there are tunable parameters (their combination creates the governor's parameter settings) that define the dynamic response of the governor. The tunable parameters for each GCS are presented in Table 1. These parameters are described in detail in the corresponding GCS description. "Variant" GCSs have one more tuning parameter than their

TABLE 1. Tunable parameters for each governor control scheme.

Governor control scheme	Tunable parameter
DB	R (p.u.)
DB_V	R (p.u.) ff_{band} (Hz)
PD	k_p k_d
PD_V	k_p k_d k_{SOC}
NLP	vtx (p.u.)
NLP_V	vtx_{max} (p.u.) f_{band} (Hz)

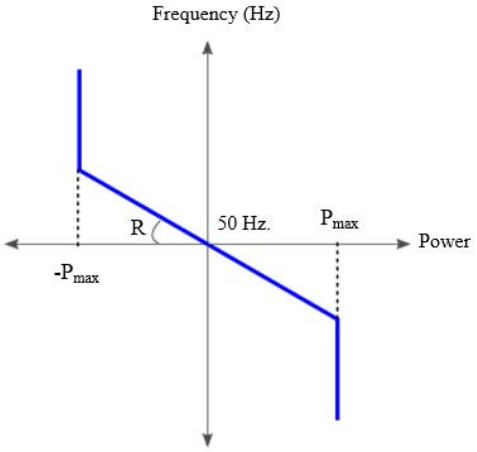

FIGURE 3. FESS DB GCS.

counterparts because they have an additional input variable related to SOC feedback.

A. DROOP BASED (DB)

The DB GCS determines the power setpoint as a function of the frequency deviation and flywheel characteristic droop (R), as expressed in (2) and graphically represented in FIGURE 3.

$$p_{FESS}\,(p.u.) = -\frac{\Delta f\,(p.u.)}{R(p.u.)} \tag{3}$$

When the frequency is higher or lower than 50 Hz, the flywheel power setpoint is proportional to the difference between the frequency value and 50 Hz. In both cases, the flywheel power was limited by its maximum electric power capacity (P_{max}).

This GCS is widely used and one of the most popular types of primary frequency regulation. This approach has been used in isolated Portuguese islands to operate a FESS plant [44].

B. DROOP BASED VARIANT (DB_V)

Similar to its one input counterpart, the DB_V GCS uses the flywheel characteristic droop (R) to determine the power setpoint. The main difference from DB is the addition of a fixed-range frequency deadband (ff_{band}) that shifts proportionally to the SOC, as shown in FIGURE 4.

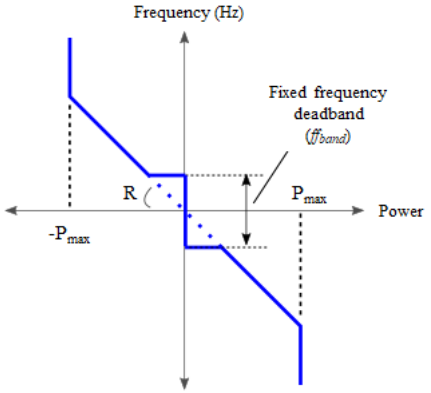

FIGURE 4. FESS DB_V GCS.

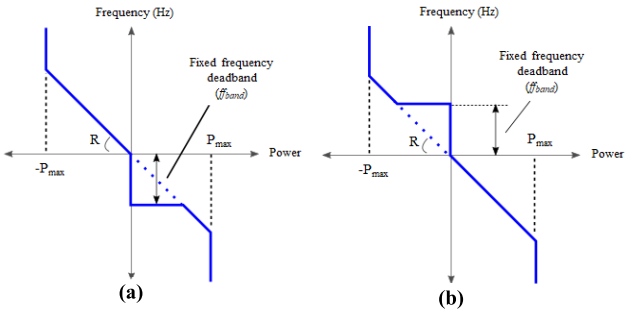

FIGURE 5. DB_V GCS behavior under different SOC values: (a) close to 0, and (b) close to 1.

The variable ff_{band} was delimited between a lower frequency ($f_{\text{low}} \leq 50Hz$) and a higher frequency ($f_{hi} \geq 50Hz$). When the SOC (in p.u.) is 0.5, the band is centered at 50 Hz. If the SOC is lower than 0.5, the band shifts downwards in proportion to the SOC value (FIGURE 5a). Otherwise, if the SOC is higher than 0.5, the band shifts upward in proportion to the SOC value (FIGURE 5b). Tunable parameters for this GCS are the R and ff_{band}.

Thus, the governor takes into consideration the flywheel SOC to establish the power setpoint, which helps improve the flywheel performance, increasing its efficiency and the flywheel lifetime by reducing the number of charging and discharging times of the FESS, as stated in [46] where this GCS is tested in a simplified GB power system model.

C. PROPORTIONAL DERIVATIVE (PD)

The PD GCS, also called the synthetic inertia control scheme, is based on a proportional derivative controller. This controller adds an additional response to the classical DB approach through a derivative action, which is proportional to the RoCoF in order to speed up the frequency regulation action.

This GCS is highly efficient for weak systems with reduced inertia, such as islanded isolated power systems. This scheme has provided good results for a FESS control in a wind-diesel power system [48], consistently smoothing the frequency deviations introduced by wind power generators.

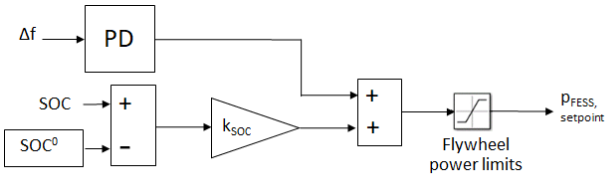

FIGURE 6. FESS PD_V GCS.

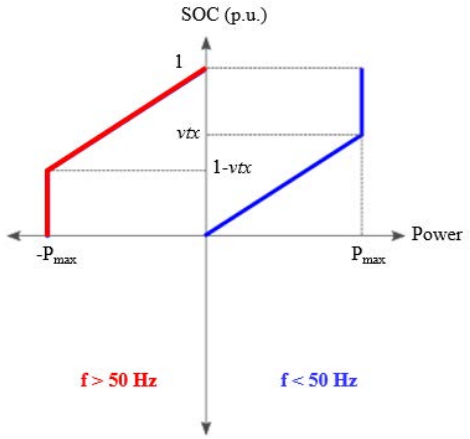

FIGURE 7. FESS NLP GCS.

The PD GCS determines the power setpoint as a function of the frequency error (Δf) and two constant parameters, k_p and k_d, which define the proportional and derivative actions of the PD controller, respectively.

D. PROPORTIONAL DERIVATIVE VARIANT (PD_V)

The PD_V working principle is similar to PD, but it has two main differences from the latter: the governor uses both the frequency and the SOC as inputs, and the SOC error (3), defined as the difference between the actual SOC (in p.u.) and 0.5, participates through a proportional controller.

$$SOC_{error} = SOC\ (p.u.) - 0.5 \tag{4}$$

The SOC error is defined in this way because when the flywheel SOC is at 0.5 p.u. it has the same capacity to absorb and inject power to the grid, making it the optimal value. This strategy, in which the SOC error participates in the governor, was adopted for a FESS in a Japanese isolated power system [49].

The PD_V GCS is composed of two different and independent controllers: a frequency PD controller that focuses on the frequency error and provides synthetic inertia and a SOC proportional controller that focuses on the SOC objective. A block diagram is presented in FIGURE 6.

As can be seen in the block diagram, both controller actions are added together in order to determine the power setpoint.

As in the previous GCS, the frequency PD controller action is determined by the k_p and k_d values, whereas the additional proportional SOC controller action is determined by the k_{SOC} value.

E. NONLINEAR PROPORTIONAL (NLP)

The NLP GCS is shown in FIGURE 7. As shown in the figure, the power setpoint varies proportionally between zero and the maximum allowed power based on the distance between the current SOC level and the fixed "vertex" (*vtx*) value. This FESS GCS has been proven to offer very good results when compared to a traditional DB GCS [50].

A detailed explanation of the working principle is presented below:

- When the frequency is lower than 50 Hz (the objective is for the FESS to supply power to the grid). If the SOC level (in p.u.) is higher than *vtx*, the power setpoint is at its maximum. However, if the SOC level is lower than *vtx*, the power setpoint is proportional to the distance between the current SOC and zero (the minimum SOC level).
- When frequency is higher than 50 Hz (objective is for FESS to absorb power from the grid), the control algorithm is similar but there are some slight differences, the change behavior point is "1 - *vtx*" and when SOC is higher than that value, power setpoint varies proportionally to distance between the current SOC and one (maximum SOC value in p.u.)

Low *vtx* values imply that the flywheel will be supplying/absorbing at maximum power most of the time, whereas high *vtx* values imply more proportional flywheel behavior.

It is also important to note that the NLP GCS considers FESS efficiency. In this way, long-term discharge of the FESS is avoided because it requires more energy to supply a specific level of power than to absorb it, owing to efficiency.

Since NLP GCS power setpoint can vary considerably when frequency switch from positive ($f > 50$Hz) to negative ($f < 50$ Hz) a frequency deadband (100 mHz) is incorporated to reduce some of the related power fluctuations.

The NLP input is mainly the SOC, as the frequency only determines whether the flywheels supply or absorb power from the grid when frequency is outside the deadband.

F. NONLINEAR PROPORTIONAL VARIANT (NLP_V)

NLP_V GCS is a singular contribution of this study. NLP_V GCS inputs, such as NLP, are both the frequency and SOC level. However, and in contrast to NLP GCS, the frequency deviation magnitude plays a major role in determining the power setpoint, efficiently making the FESS governor progressively more energetic (i.e., stronger action) according to the intensity of the frequency deviation. This smart behavior has some clear advantages over the NLP approach, presented in Section V (Analysis of Results), because the flexibility of the governor significantly reduces the wear and tear of other facilities and flywheels.

Key difference from NLP GCS is that "vertex" (*vtx*) is no longer a fixed variable. Instead, the *vtx* value varies according to the intensity of the frequency deviation, as shown in FIGURE 8.

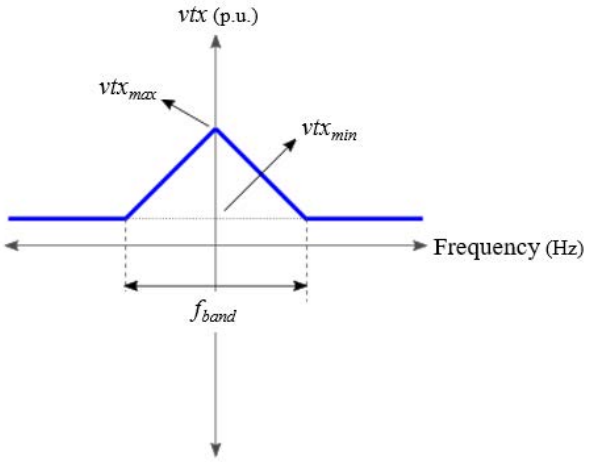

FIGURE 8. FESS NLP_V GCS.

Large frequency deviations lead to a low *vtx* value, meaning the flywheel has a higher probability of working at the rated power (if the SOC level allows it) in order to fix the frequency deviation. On the other hand, small frequency deviations lead to a bigger *vtx* value so SOC requirement to work at rated power increases. This behavior is shown in FIGURE 9.

The NLP_V governor action is defined by three parameters (FIGURE 8): the maximum vertex value (vtx_{max}), minimum vertex value (vtx_{min}), and frequency band (f_{band}) between the minimum and maximum vertex values.

Owing to the linear relationship between these variables, the *vtx* value can be obtained from the droop equation defined by these variables. Following this reasoning, this study focuses only on two of these variables for control purposes and consequently it is assumed that vtx_{min} is fixed at 0.1 (i.e., FESS power setpoint is maximum if SOC level is between 10% and 90%). In this way, governor activity (in terms of how energetic the action is) can be defined according to f_{band} and vtx_{max}. For example, when frequency deviations are very small, a large *vtx* value (which can be above one) can limit the power output of the FESS efficiently using reduced power to correct small deviations. On the other hand, when the frequency deviation amplitude is larger than the f_{band}, governor behavior will prioritize an energetic response, very close to the power setpoint limits, to reduce the frequency deviation. This mixed behavior and flexibility translates in a better SOC management over time.

A deadband (100 mHz) is also included in this GCS in order to avoid undesirable oscillations in the power injected or absorbed by the FESS.

IV. TUNING METHODOLOGY

To properly tune the parameters of the different governors (one per GCS), this study proposes the tuning methodology presented in FIGURE 10. The tuning methodology focuses on a multi-objective optimization problem and solves it using a brute-force approach based on an extensive simulation

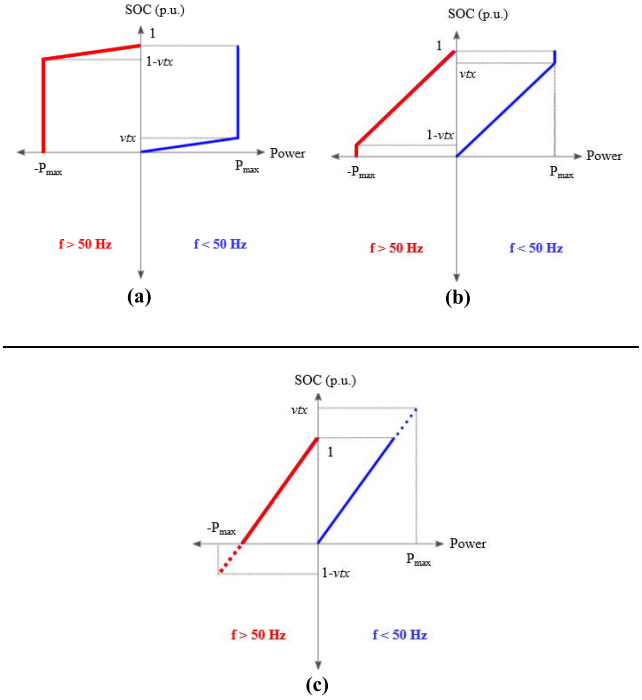

FIGURE 9. NLP_V GCS behavior under different "vertex" (*vtx*) values: (a) close to 0, (b) close to 1, and (c) above 1.

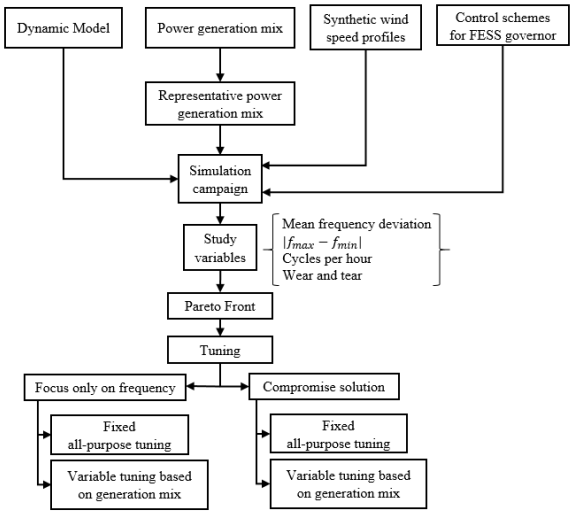

FIGURE 10. Flow chart describing the proposed tuning methodology.

campaign to obtain Pareto fronts of optimum parameter values. Because the governors' parameter settings strongly depend on the system characteristics, this tuning methodology has been applied to a model based on a case study: El Hierro isolated power system, whose main characteristics are presented in Section V.

The final objective of the proposed methodology is to obtain the best possible value for the governors' parameter settings according to different criteria, perform a multi-objective optimization based on a dataset obtained from several simulations, and extract four study variables in each simulation.

To conduct an extensive simulation campaign, it is important to develop both a realistic dynamic model and different power system generation scenarios under RE penetration. Thus, it is possible to replicate the evolution of the system over a wide operational range.

The dynamic model, explained in detail in Section II and the Appendix, paired with the different FESS GCSs, conforms to a model that replicates the system electrical frequency behavior if a FESS plant is present and its governor implements one of the control schemes discussed in Section III.

Generation mix scenarios usually depend on variable RE penetration, such as wind energy or solar energy, because they have priority to participate in energy generation when they are available and, to an extent, they define how much the other technologies participate in the operation of the power system to avoid power imbalance between generation and demand. In the El Hierro power system, the existing variable RE is the wind farm.

Variable RE not only defines the possible generation mix scenarios; it is also a source of frequency deviations due to the inherent variability of the natural resource it uses.

In the El Hierro power system, to simulate the frequency deviations caused by the VSWTs, different synthetic wind speed profiles were developed based on the historical available data and a stochastic model.

Combined with the synthetic wind speed profiles, 51 power generation mix scenarios were developed to represent the normal operating conditions of the system when wind power generators were participating. Each generation mix is based on data compiled from the local electric system operator (Red Electrica de España) [60] and defines which units and technologies (with their respective powers) are committed for the system to operate normally.

These 51 scenarios that combine different power generation configurations of the power system can be classified in groups (generation mixes) based on the main technology present in addition to the wind power during the operation of the power system, which also serves to name the groups. A total of five groups were identified. They are, from lowest to highest wind penetration: diesel (D), diesel plus hydropower (D+H), diesel plus pumping (D+P), hydropower (H) and hydraulic short circuit (HSC). The hydraulic short circuit scenario corresponds to pumps and turbines operating together, in a scenario where the power absorbed by the pumps is higher than the power injected by the Pelton turbines.

Of all the power generation configurations (generation mix scenarios) associated with each of the five identified groups, one was selected as a representative of the group. For tuning purposes, the most frequent generation mix scenarios in each of the identified groups have been selected as representative of the group. This selection is based on the configuration that has the closest values to the power demand weighted average of each group. Table 2 lists the initial power distributions for each representative generation mix. Since this study focuses on the frequency variability introduced by wind power, it has been assumed that demand is constant to properly compare the effect of FESS on frequency regulation.

TABLE 2. Initial power distribution in each representative generation mix for the power system.

Generation mix	Demand	Pumps	VSWT	Pelton Turbines	Diesel units
D	-3.40	(-)	0.15	(-)	3.25
D+H	-4.50	(-)	0.78	0.82	2.90
D+P	-4.95	-4.00	4.05	(-)	4.90
H	-6.67	(-)	4.40	2.27	(-)
HSC	-5.25	-6.00	8.23	3.02	(-)

D = diesel, D+H = diesel plus hydraulic, D+P = diesel plus pumping, H = hydraulic, HSC = hydraulic short circuit

Values are in MW. A negative value means power is consumed from the grid, and a positive value means power is injected to the grid

For each representative power generation mix scenario, five synthetic wind speed profiles were developed to represent the hypothetical evolution of the system under different wind conditions (average speed, intensity, frequency, turbulence, etc.).

In this manner, 25 simulation scenarios (five per representative power generation mix scenario) were created to tune the governor of the FESS plant for each of the GCSs proposed in Section III.

Once the simulation scenarios and the power system model has been defined, the next step in the tuning methodology is carrying out an extensive simulation campaign (brute force analysis) by slightly varying the values (in an evenly spaced predefined range) of the tunable parameters of the FESS governor from one simulation to the next for each of the 25 simulation scenarios.

Each simulation has an output of four study variables (V1-V4), forming a set of data points to conduct a multi-objective optimization of two variables.

These four study variables are the average frequency deviation AVFD (V1), difference between the Zenith and Nadir values in frequency during simulation (V2), cycles per hour of flywheels (V3), and the wear and tear (WaT) of diesel electromechanical elements and Pelton turbines nozzles (V4).

V1 and V2 are a measure of the system frequency quality (Q1), whereas V3 and V4 are a measure of the aggregated remaining lifetime of diesel units, Pelton turbines, and flywheels (Q2).

The cycles per hour of the flywheels were calculated using the rainflow counting method [61]. WaT was determined as a degradation speed by dividing the sum of the PSHP turbine nozzle positions variations (and the diesel unit equivalent) by the simulation time. The nozzle position variation is measured in per unit (p.u.) and the simulation time is measured in seconds. Consequently, the measure of the WaT variable is expressed in (p.u./s). This variable was inspired by the work of Yang *et al.* [62], [63].

When all simulations were carried out and the four study variables (V1-V4) were obtained for every simulation, a multi-variable analysis was carried out.

TABLE 3. Summary of developed tuning criteria.

	Z=Q1	$Z=\omega_1 \cdot Q1 + \omega_2 \cdot Q2$
Governor's parameter settings can change from one generation mix to another	Tuning criterion 1	Tuning criterion 2
Governor's parameter settings are fixed independently of the generation mix	Tuning criterion 3	Tuning criterion 4

The multivariable analysis was approached by a Pareto front of two condensed variables (objectives), one being Q1 and the other being Q2. Q1 and Q2 were obtained by multiplying the normalized values of their respective variables (V1 and V2 for Q1; V3 and V4 for Q2).

It is important to note that both objectives in the Pareto front are opposite because a better frequency quality implies a more intensive use of facilities with an associated reduction in the remaining lifetime of diesel units, Pelton turbines, and flywheels.

Because objectives in the Pareto front are opposite to each other, two criteria are proposed to select the best governor's parameter settings from the Pareto front: one that focuses only on improving the frequency quality (Q1) and another that proposes a compromise solution between objectives, improving the frequency quality while considering the remaining lifetime of the facilities (Q1 and Q2).

If Z is defined as the objective target and the optimized governor's parameter setting is the one that minimizes Z, then expression (5) corresponds to the first mentioned tuning criterion (focus on Q1) and expression (6) corresponds to the second mentioned tuning criterion (Q1 and Q2 objective), where ω_1 and ω_2 stand for the relative weight per unit assigned to condensed variables Q1 and Q2, respectively.

Pareto fronts are built with all possible combinations of relative weights, with ω_1 ranging from 0 to 1 with incremental steps of 0.001.

$$Z = Q1 \tag{5}$$

$$Z = \omega_1 \cdot Q1 + \omega_2 \cdot Q2; \omega_1 + \omega_2 = 1 \tag{6}$$

For each of these two criteria, two governor's parameter settings are defined: one in which the governor's parameter settings values change from one generation mix to another, and another in which there is a fixed governor's parameter settings configuration independent of the generation mix.

In this manner, four tuning criteria are made, as summarized in Table 3: focused only on Q1, with multiple configurations of governor's parameter settings according to the generation mix (tuning criterion 1) or a fixed governor's parameter setting configuration (tuning criterion 3), and focused on a compromise solution between Q1 and Q2, with multiple configurations of governor's parameter settings according to the generation mix (tuning criterion 2) or a fixed governor's parameter settings configuration (tuning criterion 4).

Table 4 shows the optimized values of these four tuning criteria options when applied to the model based on the case study of the El Hierro Island. The tuning effects and consequences are further discussed in Section V.

The search space and the incremental steps used in each of the tunable parameters to find the optimized values presented in Table 4 are specified in Table 13 of the Appendix, together with the maximum and minimum values of the studied variables (V1-V4) when the tunable parameters values are the extremes of the search space. This process allows to check that the brute force analysis can be carried out and the studied system is stable under all the range of tunable parameters values.

A. SENSITIVITY ANALYSIS

A sensitivity analysis has been performed to identify the influence each tunable parameter has on each of the studied variables that determines the governor's parameter settings. A 20% increase in each of the tunable parameters and how it affects the study variables (as a percentage) is presented in Table 5.

Cycles per hour of flywheels is the most sensitive variable for all GCSs with variations up to 16% (in NLP *vtx*), followed by the AVFD and the WaT, which are similarly sensitive in DB and PD GCSs. It is noticeable that in NLP GCSs, the AVFD is more sensitive to changes in tunable parameters than the WaT. The sensitivity analysis suggests that increasing the value of the tunable parameter usually increases the AVFD, the difference between the Zenith and Nadir frequency and the WaT, and reduces the cycles per hour. PD GCSs k_p is an exception to this rule, since its behavior is completely opposite.

V. ANALYSIS OF RESULTS

Several simulations were performed to compare different proposed GCSs and tuning criteria. These simulations were carried out using the MATLAB-Simulink model based on the El Hierro isolated power system.

A. CASE STUDY: EL HIERRO

El Hierro is an island that belongs to the archipelago of the Canary Islands. The electrical capacity of the island is 40 MW, mainly distributed in 11.18 MW provided by the DPP of Llanos Blancos, and a W-PSHP (Gorona del Viento) at a rated power of 28.82 MW.

DPP is equipped with 9 diesel generators whose power range varies from 0.67 MW to 1.9 MW. The wind farm is equipped with 5 × 2.3 MW ENERCON E-70 VSWTs. The PSHP is equipped with 4 × 2.83 MW Pelton turbines, 6 × 0.5 MW FSPs, and 2 × 1.5 MW VSPs.

This study focuses on the GCSs and governor tuning if a 200 kW FESS plant equipped with 8 × 25 kW flywheels is incorporated into the system.

El Hierro power consumption usually fluctuates between 5 MW (valley hour) and 8 MW (peak hour) on a daily basis;

TABLE 4. Values of the different governors' parameter settings based on the application of the proposed tuning criteria for each of the proposed governor control schemes.

tuning criterion[a]	generation mix	DB	DB_V	DB_V	PD	PD	PD_V	PD_V	PD_V	NLP	NLP_V	NLP_V
		R (p.u.)	R (p.u.)	ff_{band} (Hz)	K_p	K_d	K_p	K_d	K_{SOC}	vtx (p.u.)	vtx_{max} (p.u.)	f_{band} (Hz)
1	D	0.01	0.01	0.01	200	10	200	1	1	0.44	1	0.5
	D+H	0.01	0.01	0.02	200	1	200	1	1	0.1	1	0.5
	D+P	0.01	0.01	0.06	200	30	200	1	1	0.1	1	0.5
	H	0.01	0.01	0.04	200	1	200	1	1	0.1	1	0.5
	HSC	0.01	0.01	0.02	200	110	200	140	1	0.34	1.02	0.5
2	D	0.05	0.011	0.15	1	1	1	1	200	0.86	1.5	0.5
	D+H	0.018	0.018	0.15	60	1	60	1	1	0.84	1.5	0.5
	D+P	0.024	0.022	0.09	40	1	40	1	1	1.5	1.46	1.15
	H	0.033	0.03	0.09	20	1	20	1	1	1.3	1.46	1.05
	HSC	0.028	0.029	0.04	20	20	20	20	1	1.5	1.48	1.2
3	D D+H D+P H HSC	0.01	0.01	0.02	200	1	200	1	1	0.1	1	0.5
4	D D+H D+P H HSC	0.028	0.025	0.15	30	1	40	1	1	0.88	1.5	0.6

D = diesel, D+H = diesel plus hydraulic, D+P = diesel plus pumping, H = hydraulic, HSC = hydraulic short circuit

TABLE 5. Sensitivity analysis of governors tunable parameters.

	Tunable parameter		Studied variables			
	name	value	AVFD (Hz)	$f_{max} - f_{min}$ (Hz)	WaT (p.u./s)	Cycles per hour
DB DB_V	R	0.025	0.3974	2.1455	0.0363	1.2400
	ΔR	20	1.8469	1.0766	1.9337	-12.5304
	ff_{band}	0.1	0.3974	2.1455	0.0363	1.2400
	Δff_{band}	20	0.0399	-0.0013	0.0413	-0.4100
PD PD_V	k_p	100	0.4182	2.2749	0.0364	1.6267
	Δk_p	20	-1.6102	-0.7365	-2.0395	7.7077
	k_d	100	0.4182	2.2749	0.0364	1.6267
	Δk_d	20	0.4647	0.2870	0.3541	1.0891
	k_{SOC}	100	0.4182	2.2749	0.0364	1.6267
	Δk_{SOC}	20	1.4771	0.9490	1.6685	-4.0058
NLP NLP_V	vtx	1	0.3863	2.2975	0.0384	1.9382
	Δvtx	20	2.9121	1.8311	0.6159	-16.3657
	vtx_{max}	1	0.3522	2.1024	0.0353	2.6005
	Δvtx_{max}	20	2.4040	0.0543	0.0036	-10.8734
	f_{band}	1.25	0.3522	2.1024	0.0353	2.6005
	Δff_{band}	20	0.8739	0.1511	0.8256	-2.6678

Values in increments (Δ) rows are expressed as variation in % from the row above.

therefore, the capacity of the FESS plant is between 2.5% and 4% of the daily power demand.

To measure and compare the effects of the different variables that influence the FESS and the power system, this study proposes an approach based on three points: i) the GCS influence, ii) a comparison between the different tuning criteria for the governors, and iii) the generation mix influence.

The GCS influence and generation mix influence tables presented and discussed in this section have been elaborated with the arithmetic mean of all simulations conducted in this section.

Analysis of results has been elaborated with a wider range of power generation mixes and wind profiles than the tuning methodology in order to properly evaluate the differences between GCSs.

Fifteen different power generation mixes (three per technology group) have been used that include the representative power generation mix scenarios and also two less frequent scenarios for each technology group. In this manner, the behavior and response of the GCSs can be studied when the power system is operating under unusual generation mixes. The power distribution in these fifteen mixes is summarized in Table 12 of the Appendix.

For each of the 15 power generation mix scenarios considered, 50 different wind profiles have been used.

If we consider the six GCSs and the four different tuning criteria, a total of 18000 (15 generation mixes × 50 wind profiles × 6 GCSs × 4 tuning criteria) simulations have been carried out.

B. GOVERNOR CONTROL SCHEME INFLUENCE

Regardless of the GCS used, implementing a FESS plant with reduced power capacity compared to the total installed power of the system contributes significantly to frequency regulation. This contribution is greater when diesel generation groups have lower participation in the generation mix, in favor of a higher penetration of hydraulic machines (turbines and pumps) and wind generation. This is because the wind resource variability favors the appearance of frequency perturbations. Furthermore, the penstock length makes hydraulic units (i.e., turbines and pumps) regulation of the frequency generate more ripple than when the frequency regulation is provided by diesel units. This combined effect, which will be discussed later when addressing the influence of the generation mix, is shown in FIGURE 16.

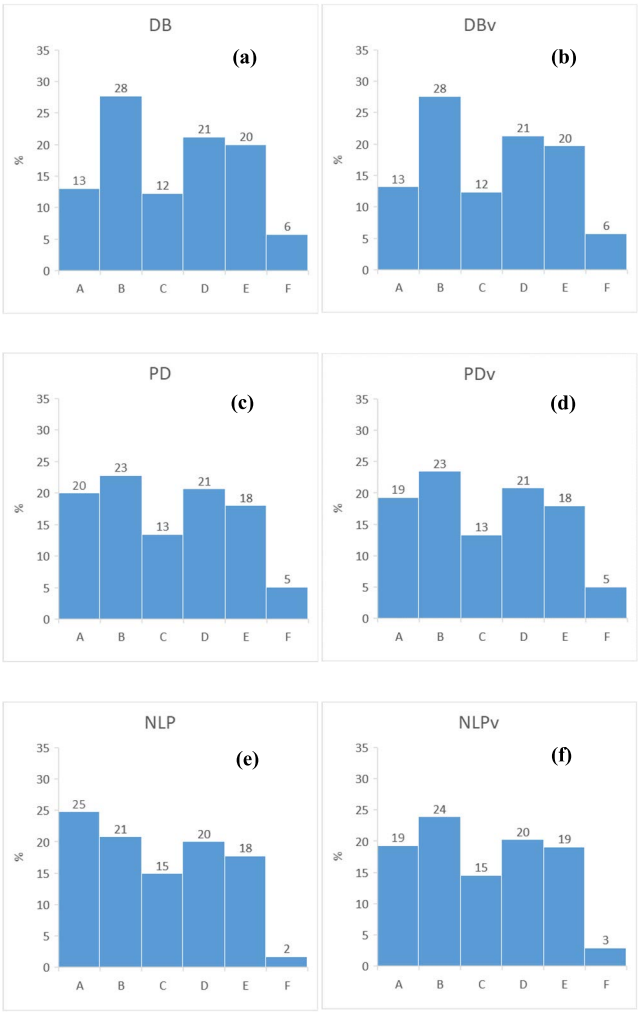

FIGURE 11. Histograms based on AVFD of all generation scenarios studied in each GCS with a tuning criterion based on best frequency response (Tuning criterion 1). Y axis values are presented as a percentage. X axis intervals, expressed in Hz are A = [0,0.15] B = (0.15,0.3] C = (0.3,0.45] D = (0.45,0.6] E = (0.6,0.75] F => 0.75.

Comparisons between GCSs, numerically presented in the tables in this section (Table 6, Table 7, Table 8 and Table 9), were performed by comparing the same study variables as in Section IV (V1-V4) with the addition of the average FESS SOC level.

To illustrate the GCS influence and compare GCSs between them, this subsection focuses on the graphics and results derived from the application of tuning criterion 1, which means that the main objective is to obtain the best frequency quality (Q1), and the governor's parameter settings can change from one representative generation mix to another.

In order to have a general view of the differences between one GCS and another, if we focus, for example, only on the AVFD, presented in the form of histograms (FIGURE 11), we can observe some clear differences. PD GCSs improve DB GCSs by reducing the AVFD, specifically when the AVFD is low (the bar 'A' and 'B' exchange 5% when going from DB to PD). NLP GCSs, since they are the most aggressive

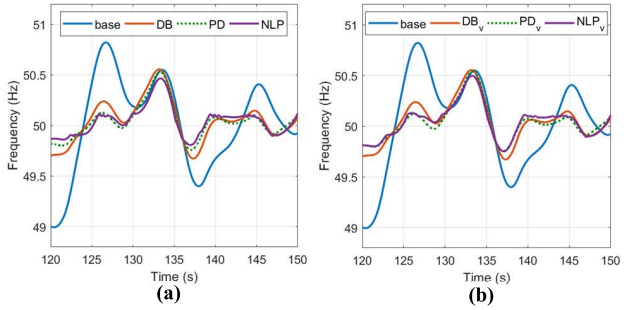

FIGURE 12. System frequency evolution with DB, PD, NLP GCSs (a) and with DB$_V$, PD$_V$, NLP$_V$ (b) GCSs in an hydro generation mix scenario: wind (4.4MW), hydro (2.27MW), pumping (0MW), diesel units (0MW), demand (6.67MW) with a tuning criterion based on best frequency response (Tuning criterion 1).

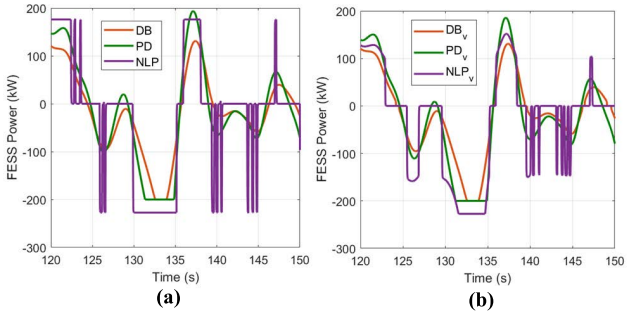

FIGURE 13. FESS power evolution with DB, PD, NLP GCSs (a) and with DB$_V$, PD$_V$, NLP$_V$ (b) GCSs in an hydro generation mix scenario: wind (4.4MW), hydro (2.27MW), pumping (0MW), diesel units (0MW), demand (6.67MW) with a tuning criterion based on best frequency response (Tuning criterion 1).

GCSs, manage to reduce the higher AVFD (notable in the reduction of the rightmost bar 'F'). There are few differences in the same principle based GCSs for DB-DB$_V$ and PD-PD$_V$ respectively, but there are some differences for NLP and NLP$_V$.

Focusing on the graphical evolutions of frequency (FIGURE 12), FESS power exchange (FIGURE 13), and SOC level (FIGURE 14), it is clear that the GCSs and their associated governors' parameter settings have enough influence to produce noticeable differences.

The largest differences are found between NLP – NLP$_V$ GCSs and the rest, as can be seen, for example, in FIGURE 13, where NLP GCS makes FESS work near the maximum power output with strong variations in small frames of time. This behavior also translates to a larger frequency impact (FIGURE 12). According to Table 6, and referenced to the base case (no FESS), NLP and NLP$_V$ GCSs reduce AVFD by 29% and 26%, respectively, whereas DB and DB$_V$ GCSs reductions are both 22%, and PD and PD$_V$ GCSs reductions are both 25%.

NLP GCS offers the best results in terms of frequency regulation but worse values in WaT than PD GCS (up to 2.5%). This effect occurs because the NLP GCS is very energetic in its control action: the power output (i.e., both charging and discharging) is maximum (FIGURE 13) when the SOC is between a set interval defined by the *vtx* variable.

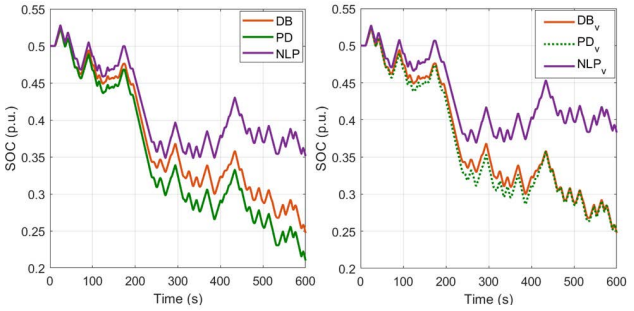

FIGURE 14. FESS SOC evolution with DB, PD, NLP GCSs (a) and with DB$_V$, PD$_V$, NLP$_V$ (b) GCSs in an hydro generation mix scenario: wind (4.4MW), hydro (2.27MW), pumping (0MW), diesel units (0MW), demand (6.67MW) with a tuning criterion based on best frequency response (Tuning criterion 1).

As expected of a very energetic governor, the NLP GCS has the highest cycles per hour value of all the GCSs. However, considering the cycles guaranteed by flywheel manufacturers, NLP GCS would not cause an appreciable reduction in the flywheel lifetime [35], [64], [65].

Compared to NLP, NLP$_V$ GCS behavior is less energetic because the magnitude of the frequency deviation plays an important role in determining the power setpoint (FIGURE 13). This smart behavior allows smooth and partial elimination of the high frequency ripple associated with NLP GCS (FIGURE 12).

In this manner, the NLP$_V$ GCS reduces WaT by an additional 0.87% over NLP, for a total of 21.43% over the base case (situating itself in a middle position between DB and PD), with 0.2 less flywheel cycles per hour, the second best frequency results and increasing the average SOC level to 47.1%, whereas the NLP average SOC level is 46.2%.

Even though the NLP and NLP$_V$ GCSs present the most differences, analyzing and comparing the other GCSs also offer some interesting results.

The DB GCS offers the least improvement in frequency quality, and there are only slight differences between DB and DB$_V$ GCSs, as can be seen graphically in FIGURE 12, and numerically in Table 6, where value differences from DB GCS to DB$_V$ GCS are less than 1%.

The PD GCS, by adding synthetic inertia, offers a better dynamic response to sudden changes in frequency than the DB GCS (FIGURE 12) and this translates, according to Table 6, into a lower AVFD (−3%) and it is also the best GCS for reducing the WaT (−3%) since it offers a very fast regulation that reduces the regulation effort offered by Pelton turbines and diesel groups. These differences are more noticeable in the generation mix scenarios where hydro and wind have a higher presence than diesel groups, owing to an increase in frequency oscillations, increasing RoCoF, and making the FESS synthetic inertia offered by the PD GCS more relevant. The downside of the PD GCS over the DB GCS is that its frequency action is more energetic, especially when frequency oscillations are very common. According to Table 6, the PD GCS has more cycles per hour (+0.48) than the DB GCS. The average SOC is also worse in PD GCS than in DB GCS (−1.9%) because PD GCS does not take into consideration the SOC of the flywheel in its control scheme.

TABLE 6. Studied variables values with tuning criterion 1 based on best frequency quality response with governor's parameter settings changing in each generation mix.

GCS[a]	Avg. Frequency deviation (Hz)	$f_{max} - f_{min}$ (Hz)	Wear and tear[b] (p.u./s)	Cycles per hour	Average SOC (%)
BC	0.51±0.02	3.07±0.11	4.14±0.17	-	-
DB	-21.98±3.15	-16.48±3.03	-20.22±3.73	2.19±0.06	42.65±0.43
DB$_V$	-22.19±3.14	-16.48±3.03	-20.21±3.73	2.18±0.06	42.67±0.43
PD	-25.29±3.16	-15.52±3.08	-22.98±3.73	2.67±0.05	40.75±0.43
PD$_V$	-25.12±3.16	-15.43±3.08	-22.89±3.74	2.65±0.05	41.97±0.38
NLP	-29.15±3.01	-15.00±3.08	-20.56±3.64	2.71±0.06	46.23±0.37
NLP$_V$	-26.11±3.06	-15.69±3.07	-21.43±3.68	2.51±0.06	47.11±0.30

[a]Governor control scheme: BC = base case, DB = droop based, DB$_V$ = droop based variant, PD = proportional derivative, PD$_V$ = proportional derivative variant, NLP = nonlinear proportional, NLP$_V$ = nonlinear proportional variant

[b]Wear and tear is expressed as the speed of degradation in 1×10^{-2} p.u./s.

[c]Values are expressed as variation in % from the base case, whereas cycles per hour and average SOC are expressed as their real values. All values are expressed with confidence intervals using an alpha value of 0.05.

The advantage of the PD$_V$ GCS over the PD GCS is SOC recovery (i.e., maintaining a 50% SOC level) because of the introduction of SOC feedback in the control loop, while maintaining almost constant the rest of the study variables. The SOC behavior improvement can be observed in FIGURE 14, where the evolution of the SOC of the PD$_V$ GCS is better than that of the PD GCS. Numerically, in Table 6, the average SOC value of the PD$_V$ GCS is 1.22% higher than PD GCS. The differences between PD$_V$ and PD GCSs in the other study variables are negligible, as observed in the AVFD (25.1% and 25.3% reduction over the base case, respectively) or WaT (22.9% and 23%, respectively).

It is also interesting to highlight that SOC recovery in NLP and NLP$_V$ GCSs (FIGURE 14) is noticeably better than in the other GCSs (between 3% and 6% better), while maintaining very similar cycles per hour.

This is due to NLP based GCSs adding FESS efficiency in their control loops.

C. TUNING CRITERIA INFLUENCE

To effectively determine if the tuning criteria have an influence on the results, different comparisons were made: i) comparison between criteria with the same objective (compare tuning criteria 1 vs. 3; and 2 vs. 4) and ii) comparison between criteria with different objectives (comparing tuning criteria 1 vs. 2 and 3 vs. 4).

Comparing tuning criteria 1 vs. 3 (i.e., only frequency-oriented tuning), the results (Table 6 vs. Table 8) show very slight differences because there are very few changes in the governors' parameter settings configurations (Table 4). Based on this, it is safe to assume that when the main objective is to reduce the AVFD, there is no need to change the governor's parameter settings from one generation mix to another, because the improvement is minimal.

TABLE 7. Studied variables values with tuning criterion 2 based on compromise solution with governor's parameter settings changing in each generation mix.

GCS[a]	Avg. Frequency deviation (Hz)	$f_{max} - f_{min}$ (Hz)	Wear and tear[b] (p.u./s)	Cycles per hour	Average SOC (%)
BC	0.51±0.02	3.07±0.11	4.14±0.17	-	-
DB	-14.03±3.40	-15.93±2.88	-12.48±3.96	1.27±0.05	45.30±0.31
DB_V	-15.81±3.38	-16.72±2.90	-14.79±3.86	1.46±0.04	44.78±0.36
PD	-10.51±3.63	-12.68±3.04	-9.44±4.10	0.96±0.04	46.49±0.27
PD_V	-10.37±3.64	-12.58±3.05	-9.33±4.10	0.94±0.04	47.66±0.18
NLP	-14.15±3.67	-8.26±3.32	-10.42±4.12	1.25±0.02	48.70±0.12
NLPV	-21.76±3.18	-17.00±3.00	-18.61±3.80	2.00±0.05	47.88±0.23

TABLE 8. Studied variables values with tuning criterion 3 based on best frequency quality response with a fixed governor's parameter settings configuration.

GCS[a]	Avg. Frequency deviation (Hz)	$f_{max} - f_{min}$ (Hz)	Wear and tear[b] (p.u./s)	Cycles per hour	Average SOC (%)
BC	0.51±0.02	3.07±0.11	4.14±0.17	-	-
DB	-21.98±3.15	-16.48±3.03	-20.22±3.73	2.19±0.06	42.65±0.43
DB_V	-22.20±3.14	-16.48±3.03	-20.22±3.73	2.19±0.06	42.66±0.43
PD	-25.32±3.16	-15.49±3.08	-22.75±3.75	2.68±0.05	40.75±0.43
PD_V	-25.20±3.15	-15.39±3.08	-22.66±3.75	2.66±0.05	41.96±0.38
NLP	-29.26±3.01	-15.04±3.08	-20.60±3.63	2.72±0.06	46.12±0.38
NLPV	-26.12±3.06	-15.69±3.07	-21.43±3.68	2.52±0.06	47.11±0.30

TABLE 9. Studied variables values with tuning criterion 4 based on compromise solution with a fixed governor's parameter settings configuration.

GCS[a]	Avg. Frequency deviation (Hz)	$f_{max} - f_{min}$ (Hz)	Wear and tear[b] (p.u./s)	Cycles per hour	Average SOC (%)
BC	0.51±0.02	3.07±0.11	4.14±0.17	-	-
DB	-14.25±3.36	-16.45±2.84	-12.66±3.93	1.26±0.04	45.23±0.31
DB_V	-15.32±3.30	-16.69±2.86	-13.63±3.90	1.35±0.05	45.00±0.33
PD	-12.68±3.44	-15.75±2.83	-11.08±3.99	1.09±0.04	45.83±0.27
PD_V	-15.13±3.33	-16.57±2.87	-13.62±3.90	1.35±0.05	46.45±0.22
NLP	-17.89±3.45	-10.41±3.21	-13.52±3.97	1.63±0.03	48.42±0.14
NLPV	-23.49±3.08	-16.58±3.04	-20.26±3.70	2.19±0.06	47.67±0.27

Comparing tuning criteria 2 vs. 4 (i.e., compromise solution tuning), the results change noticeably; for example, the AVFD reduction over the base case for NLP GCS increases from 14.1% in criterion 2 to 17.9% in criterion 4 (Table 7 vs. Table 9).

A compromise solution between objectives (frequency quality Q1 and facilities remaining lifetime Q2) yields more variation in results because the Q2 objective is very sensitive to changes in the governor's parameter settings (specifically cycles per hour as discussed in the sensitivity study in Section IV). For example, NLP GCS WaT reduction over the base case changed from 10.42% in criterion 2 to 13.52% in criterion 4.

The most notable differences from Table 7 to Table 9 (criteria 2 and 4, respectively) are found in cycles per hour as it is the most sensitive studied variable, followed by the WaT and AVFD. Going from a mix oriented tuning (tuning criterion 2) to a more overall oriented tuning (tuning criterion 4) for PD and NLP based GCSs increases the flywheels cycles per hour, but also improves the WaT and the AVFD. As an example, the NLP GCS values vary from Table 7 to Table 9 in 3.74% in AVFD, 3.10% in WaT, and 0.38 in cycles per hour.

DB based GCSs, on the other hand, have only slight changes, and their associated studied variables values are almost constant.

The results are also more sensitive to governors' parameter settings depending on which GCS is selected, as it was discussed in the sensitivity study in Section IV. The variations in the results are related to how energetic the governor is when it comes to frequency regulation. The more energetic a governor is (i.e., going down in tables from DB to NLP GCSs), the more noticeable the difference becomes. This behavior can justify, for example, that when using NLP GCS, it could be worth changing the governor's parameter settings when moving from one generation mix to another, using a tuning criterion of 1 or 2.

Finally, when comparing tuning criteria with different objectives for the same GCS: tuning criteria 1 vs. 2 (Table 6 vs. Table 7) and tuning criteria 3 vs. 4 (Table 8 vs. Table 9), respectively, strong differences can be found, as can be graphically seen in FIGURE 15, which shows the NLP GCS response under different tuning criteria for the governor's parameter settings. This is expected because different objectives usually have very different governors' parameter settings, as summarized in Table 4. The most noticeable difference is associated with the NLP governor (the most energetic GCS), where switching from a compromise solution objective (Q1+Q2) with tuning criterion 2 to an only frequency quality objective (Q1) with tuning criterion 1, reduces the AVFD by 15%; however, the flywheel cycles per hour increase by 1.46, and the SOC average value is reduced by 2.47% (Table 6 vs. Table 7).

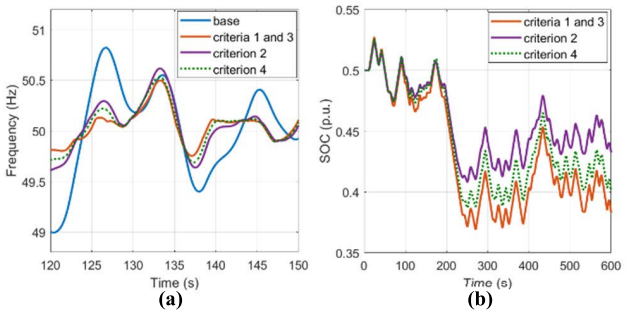

FIGURE 15. Power system frequency (a) and FESS SOC (b) evolution in a hydro generation mix scenario: wind (4.4MW), hydro (2.27MW), pumping (0MW), diesel units (0MW), demand (6.67MW) under different tuning criteria for a NLP_V GCS. Tuning criteria match the Table 3 definition and the governor's parameter settings values of Table 4.

D. GENERATION MIX INFLUENCE

Independently of the selected generation mix scenario, the FESS installation reduces the frequency deviations of the power system. However, the impact of the FESS is limited

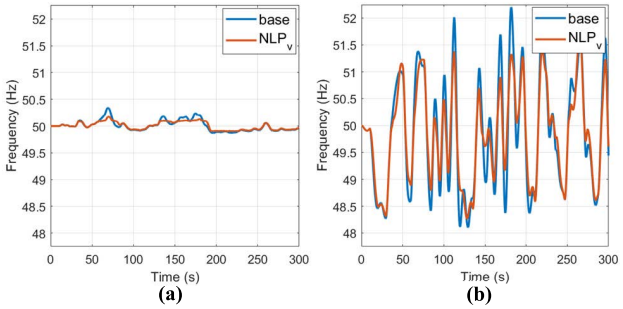

FIGURE 16. Power system frequency evolution without FESS plant (base case) and with FESS plant (NLP_V GCS) with a tuning criterion 1 in a representative diesel generation mix (a) and in a representative hydraulic short circuit generation mix (b).

when diesel groups play a larger role in the generation mix than renewable energies (PSHP and wind farm). As stated in this section, penstock length causes an increase in frequency oscillations when hydropower units (pumps and/or Pelton turbines) operate, and wind resource variability also introduces frequency deviations. These two effects translate to the FESS fast frequency response utility being greater in smoothing the system frequency when one of these effects or both are present.

This contrast is graphically shown in FIGURE 16 where frequency deviations in the representative diesel generation mix scenario are less frequent and have less amplitude than in the representative HSC generation mix scenario. In a representative diesel generation mix scenario without FESS regulation, the frequency maximum deviations are less than 0.5 Hz (FIGURE16a) and the FESS effect is reduced because the frequency is already very smooth. In a representative HSC generation mix scenario, the frequency can deviate up to 2 Hz (FIGURE16b) from the reference frequency (50 Hz) without FESS participation, and the FESS can effectively smooth peak frequencies by 0.5 Hz.

We can contrast this graphical information with the numerical values. According to Table 10, where the AVFD under tuning criterion 1 for the five representative generation mixes and GCSs is summarized, if we focus on the base case (first row), in a wind plus diesel (D) generation mix scenario, the AVFD is 59 mHz, whereas in the wind plus HSC generation mix scenario, the AVFD is 889 mHz.

As expected, if we analyze, for example, the NLP_V GCS impact on these two scenarios, NLP_V GCS reduces the AVFD by 5 mHz (reaching an AVFD of 54 mHz) in a diesel generation mix scenario and by 192 mHz (reaching an AVFD of 697 mHz) in a HSC generation mix scenario.

This contrast makes it clear that the FESS impact is larger when frequency oscillations are more frequent and have more amplitude, as in high RE penetration scenarios, where wind and hydro generation play a major role.

It is also important to note that high RE and high frequency oscillations can also be present (albeit less frequently) in diesel based generation mix scenarios. In Table 11, all 15 studied generation mix scenarios have been considered, and they have the same percentage of occurrence. The results

TABLE 10. Mean Frequency Deviation of representative mixes with tuning criterion 1 based on best frequency quality response with governor's parameter settings changing in each generation mix.

GCS[a]	D	D+H	D+P	H	HSC
BC[b]	5.92±0.4	18.46±0.59	37.71±0.75	85.87±1.12	88.94±1.34
DB[c]	4.64±0.31	14.64±0.45	31.67±0.66	65.01±1.19	71.88±1.28
DB_V[c]	4.64±0.31	14.62±0.45	31.60±0.66	64.83±1.19	71.61±1.27
PD[c]	3.84±0.25	12.77±0.42	30.06±0.68	63.23±1.24	70.64±1.36
PD_V[c]	3.87±0.26	12.87±0.42	30.09±0.68	63.29±1.24	70.80±1.36
NLP[c]	5.33±0.28	12.29±0.31	27.78±0.65	60.02±1.27	68.45±1.35
NLP_V[c]	5.38±0.3	13.3±0.37	29.62±0.66	62.17±1.24	69.71±1.31

D = diesel, D+H = diesel plus hydraulic, D+P = diesel plus pumping, H = hydraulic, HSC = hydraulic short circuit

[a]Governor control scheme: BC = base case; DB = droop based DB_V = droop based variant, PD = proportional derivative, PD_V = proportional derivative variant, NLP = nonlinear proportional, NLP_V = nonlinear proportional variant.

[b]Base Case values are in 1×10^{-2} Hz

[c]Values are expressed as variation in % from the base case with confidence intervals using an alpha value of 0.05.

TABLE 11. Mean Frequency Deviation of all generation mixes with tuning criterion 1 based on best frequency quality response with governor's parameter settings changing in each generation mix.

GCS[a]	D	D+H	D+P	H	HSC
BC[b]	29.52±3.58	39.01±3.48	37.99±2.00	68.61±5.20	83.46±1.66
DB[c]	23.42±2.77	30.20±2.60	31.89±1.83	49.15±3.76	67.07±1.51
DB_V[c]	23.37±2.76	30.14±2.60	31.81±1.83	49.03±3.75	66.82±1.52
PD[c]	21.89±2.71	28.23±2.59	30.23±1.88	47.05±3.79	65.78±1.56
PD_V[c]	21.95±2.71	28.30±2.58	30.25±1.87	47.15±3.79	65.95±1.55
NLP[c]	21.13±2.46	26.23±2.39	28.45±1.9	44.15±3.54	63.22±1.61
NLP_V[c]	22.09±2.56	28.01±2.5	29.86±1.87	46.35±3.64	64.73±1.56

are considerably different in only diesel scenarios and diesel plus hydroelectric scenarios when compared to representative generation mix scenarios (Table 10). The cause of this contrast is that these mixes (D and D+H) are rarely used under high wind power penetration, and in such cases, wind power is higher than diesel, increasing frequency deviations by a combination of increased wind variability and reduced system inertia.

This behavior takes into consideration the generation mix scenario as an important decision when selecting the best GCS. For example, in very high RE scenarios with wind and hydro penetration, such as hydro and HSC, it is worth considering a very energetic GCS, such as NLP, NLP_V, or even PD_V, whereas in scenarios where diesel is more present, other GCSs or governor's parameter settings can be considered.

VI. CONCLUSION

The main objective of this study is to compare six different governor control schemes (GCSs) of a FESS in an isolated power system with a high penetration of renewables. Of these six GCSs, the first four (DB, DB_V, PD, and PD_V) are based on a bibliography review, whereas NLP GCS has been developed by the same investigation team and NLP_V GCS is a contribution of this study. Furthermore, a methodology is proposed to tune these governors and used under different tuning criteria to compare results, analyzing the contribution to reducing

the impact of increased penetration of RE into the system frequency.

To compare the different GCSs, different representative scenarios of the power mix generation and wind speed profiles were defined. Each GCS was used in every power system representative generation mix scenario previously stated under different tuning criteria. The methodology to estimate the best governor's parameter settings for each GCS under different objectives focuses either only on reducing frequency deviations or on a compromise solution between reducing frequency deviations and improving the remaining lifespan of facilities participating in frequency regulation. These GCSs and their associated tuning criteria have been checked in the El Hierro power system (Spain); therefore, a realistic dynamic model of this isolated power system has been developed in MATLAB-Simulink, including a wind farm, PSHP, FESS, DPP, and AGC responsible for frequency secondary regulation services.

Based on the results obtained, the dynamic response of the system is different as a function of the GCS and the tuning criteria, and these differences are sufficient to justify the use of one GCS or another based on which objective or objectives are more important. Considering SOC as an input in the GCS (PD_V and NLP_V) implies a continuous recovery of the SOC and does not have a significant negative impact on the rest of the analyzed system variables.

With regard to GCSs, the NLP and NLP_V governor action on frequency is very energetic, and therefore, FESS operates close to its power limit. In this way, NLP and NLP_V GCSs manage to reduce the AVFD by up to 29% and 26%, respectively, but it also implies minor improvement in WaT over the other GCSs (especially the NLP GCS) and an increase in flywheels cycles per hour in comparison with classical PD or DB GCSs. Nonetheless, the cycles per hour values associated with NLP and NLP_V GCSs are compatible with the manufacturers' lifespan (20 years).

The tuning criteria have a relevant influence on the results. Taking into account the WaT of conventional units and flywheels cycles per hour in the tuning process involves changes in governors' parameter settings. In this case study, the numerical results suggest that it may be worth modifying governors' parameter settings according to the power mix generation while keeping them constant if the tuning criteria only consider frequency deviations.

As a general overview, it can be stated that including a FESS, even if its capacity is reduced compared to the total power system, contributes significantly to improving the frequency regulation as well as reducing the WaT.

APPENDIX A
MODEL EQUATIONS NOMENCLATURE

A_r	Area swept by rotor Blades [m^2].
a_w	Wave speed [m/s].
$c_{h,k}$,$b_{h,k}$,$a_{h,k}$	Coefficients of pump characteristic function.
C_p	Variable-speed wind turbine (VSWT) power coefficient.
$c_{p,k}$,$b_{p,k}$,$a_{p,k}$	Coefficients of pump characteristic function.
Ec	FESS stored kinetic energy [J].
f	Frequency [p.u.].
f_{ref}	Reference frequency [p.u.].
g	Gravity acceleration [m/s^2].
h	Net head [p.u.].
H_b	Base head [m].
h_i	Head at the end of the $i^{th}\Pi$ element of the penstock [p.u.].
H_w	Wind turbine inertia constant [p.u.].
I	FESS moment of inertia [kg·m^2].
J_k	Rotor pump inertia [s].
$K_{i\omega}$	integral gain of VSWTs speed control loop.
$K_{p\omega}$	proportional gain of VSWTs speed control loop.
K_u	Participation factor on AGC.
L	Penstock length [m].
$n_{nom,k}$	Nominal rotational speed of each pump [p.u.].
$N_{nom,k}$	Nominal rotational speed of each pump [r.p.m.].
$n_{p,k}$	Rotational speed of each pump [p.u.].
$n_{p,k}$	Rotational speed of each pump [p.u.].
N_{syn}	Synchronous speed [r.p.m.].
n_t	Number of segments in which the penstock is divided.
P_b	Base power [MW].
$p_{H,j}$	Power supplied by each turbine [p.u.].
$p_{pe,k}$	Power consumed by each pump [p.u.].
$p_{pm,k}$	Mechanical power of each pump [p.u.].
p_w	power supplied by the wind farms [p.u.].
p_{wm}	Wind mechanical power [p.u.].
p_w^0	initial power supplied by the wind farms [p.u.].
q_j	Flow through each turbine [p.u.].
Q_b	Base Flow [m^3/s].
q_i	Flow at the end of the $i^{th}\Pi$ element of the penstock [p.u.].
$q_{p,k}$	Flow pumped by each pump [p.u.].
r/2	Continuous head loss coefficient in the penstock [p.u.].
S	Penstock section [m^2].
s_{nom}	Electrical machine slip.
s_w	Wind speed [m/s].
T	FESS torque [N·m].
T_e	Water elastic time (L/a_w).
T_r	Hydro governor dashpot time constant [s].
T_u	Acting secondary regulation time [s].
T_w	Penstock water starting time [s].
z_j	Nozzle opening of each turbine [p.u.].
δ	Hydro governor temporary speed droop.
ΔRR	Total secondary regulation effort.
ρ	Air density: 1.225 kg/m^3.

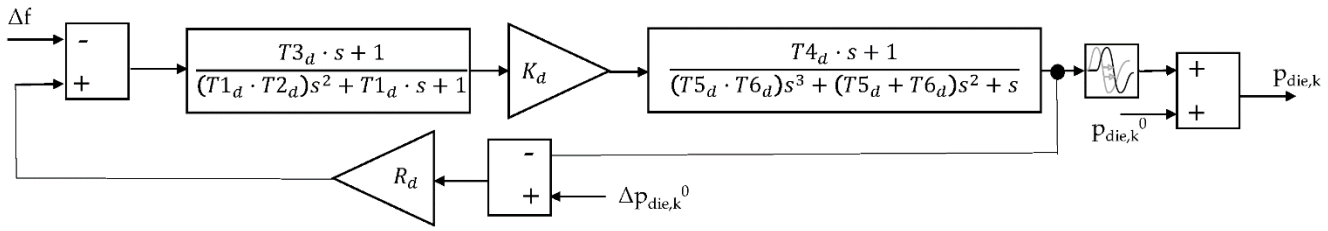

FIGURE 17. Transfer function of one diesel group.

ω VSWT rotational rotor speed [p.u.].
ω_{FESS} FESS rotational speed [rad/s].
ω_{ref} reference VSWT rotational rotor speed [p.u.].

APPENDIX B
MODEL EQUATIONS

Variable speed wind turbines equation

$$p_w = p_w^0 + \omega\left[K_{p\omega} + K_{i\omega}\int dt\right](\omega - \omega_{ref}) \tag{7}$$

$$p_{wm} = \frac{\rho}{2}A_r s_w^3 C_p / P_b \tag{8}$$

$$\frac{d\omega}{dt} = \frac{1}{2H_w}\frac{1}{\omega}(p_{wm} - p_w) \tag{9}$$

$$\omega_{ref} = -0.75p_w^2 + 1.59p_w + 0.63 \tag{10}$$

Automatic Generation Control equations

$$\Delta RR = -\Delta f \cdot \mathrm{K}_f \tag{11}$$

$$\Delta p_{H,j}^{ref} = \frac{1}{T_{u,H}}\int \Delta RR \cdot K_{u,H,j}dt \tag{12}$$

$$\Delta p_{DG,m}^{ref} = \frac{1}{T_{u,DG}}\int \Delta RR \cdot \mathrm{K}_{u,DG,m}dt \tag{13}$$

$$\sum \mathrm{K}_u = \sum_1^j \mathrm{K}_{u,H,j} + \sum_1^m \mathrm{K}_{u,DG,m} = 1 \tag{14}$$

Pelton turbines equations

$$q_j = z_j\sqrt{h} \tag{15}$$

$$p_{H,j} = q_j f\left(2\sqrt{h} - f\right) \tag{16}$$

$$\Delta z_j = \left[\frac{1}{\delta} + \frac{1}{\delta T_r}\int dt\right](f_{ref} - f) \tag{17}$$

Penstocks equations

$$\frac{dh_i}{dt} = n_t\frac{T_w}{T_e^2}(q_i - q_{i+1}) \tag{18}$$

$$\frac{dq_i}{dt} = \frac{n_t}{T_w}\left(h_i - h_{i+1} - \frac{r}{2n_t}q_i|q_i|\right) \tag{19}$$

$$T_w = \frac{L}{gS}\frac{Q_b}{H_b} \tag{20}$$

Pumps equations

$$h_{n,k} = \left(c_{h,k} \cdot q_{p,k}^2 + b_{h,k} \cdot q_{p,k} + a_{h,k}\right)\left(\frac{n_{p,k}}{n_{nom,k}}\right)^2 \tag{21}$$

$$p_{pm,k} = \left(c_{p,k} \cdot q_{p,k}^2 + b_{p,k} \cdot q_{p,k} + a_{p,k}\right)\left(\frac{n_{p,k}}{n_{nom,k}}\right)^2 \tag{22}$$

$$p_{pe,k} = \frac{1 - \frac{n_{p,k}}{f}}{s_{nom}}\frac{N_{syn}}{N_{nom,k}} \tag{23}$$

$$n_{p,k}\frac{dn_{p,k}}{dt} = \frac{1}{J_k}\left(p_{pe,k} - p_{pm,k}\right) \tag{24}$$

Flywheel equations

$$E_c = \frac{1}{2} \cdot I \cdot \omega_{FESS}^2 \tag{25}$$

$$\frac{d\omega_{FESS}}{dt} = \frac{1}{I}\left(\pm T_{charge/discharge} - T_{autodischarge}\right) \tag{26}$$

TABLE 12. Initial power distribution in each generation mix for the power system.

Generation mix	Demand	Pumps	VSWT	Pelton turbines	Diesel units
D	**-3.40**	**(-)**	**0.15**	**(-)**	**3.25**
D	-6.22	(-)	1.07	(-)	5.15
D	-6.67	(-)	4.40	(-)	2.27
D+H	**-4.50**	**(-)**	**0.78**	**0.82**	**2.90**
D+H	-6.22	(-)	1.07	3.71	1.44
D+H	-6.05	(-)	3.14	1.04	1.87
D+P	**-4.95**	**-4.00**	**4.05**	**(-)**	**4.90**
D+P	-4.50	-0.50	0.78	(-)	4.22
D+P	-6.11	-6.00	6.93	(-)	5.18
H	**-6.67**	**(-)**	**4.40**	**2.27**	**(-)**
H	-5.35	(-)	0.62	4.73	(-)
H	-4.79	(-)	3.02	1.77	(-)
HSC	**-5.25**	**-6.00**	**8.23**	**3.02**	**(-)**
HSC	-4.30	-2.80	3.70	3.40	(-)
HSC	-6.10	-4.80	6.70	4.20	(-)

D = diesel, D+H = diesel plus hydraulic, D+P = diesel plus pumping, H = hydraulic, HSC = hydraulic short circuit

Values are in MW. A negative value means power is consumed from the grid, and a positive value means power is injected to the grid. Representative generation mix scenarios are presented in **bold** letters.

APPENDIX C
AUXILIARY INFORMATION

See Table 12 and Table 13.

TABLE 13. Incremental step, maximum values and minimum values of the studied variables for the tunable parameters limit values in each of the governor control schemes.

GCS	tunable parameters	Incremental step Δ used for brute force analysis	AVFD (Hz)		$f_{max} - f_{min}$ (Hz)		WaT (p.u./s)		Cycles per hour	
			min	MAX	min	MAX	min	MAX	min	MAX
DB	$R_m = 0.01$ $R_M = 0.05$	ΔR=0.001	0.0378 0.0449	0.7348 0.8354	0.3178 0.3845	4.1875 4.1806	0.0029 0.0038	0.0690 0.0788	0.3061 0.0771	3.3134 1.3749
DB_V	R_m=0.01, $ff_{band,m}$=0.01 R_m=0.01, $ff_{band,M}$=0.15 R_M=0.05, $ff_{band,m}$=0.01 R_M=0.05, $ff_{band,M}$=0.15	ΔR=0.001 Δff_{band}=0.01	0.0377 0.0426 0.0449 0.0459	0.7335 0.7320 0.8343 0.8335	0.3178 0.3209 0.3845 0.3843	4.1875 4.1875 4.1806 4.1804	0.0029 0.0034 0.0038 0.0039	0.0690 0.0690 0.0788 0.0788	0.3053 0.1266 0.0771 0.0408	3.3133 3.2930 1.3749 1.3725
PD	$k_{p,m}$=1, $k_{d,m}$=1 $k_{p,m}$=1, $k_{d,M}$=200 $k_{p,M}$=200, $k_{d,m}$=1 $k_{p,M}$=200, $k_{d,M}$=200	Δk_p=10 Δk_d=10	0.0470 0.0485 0.0316 0.0317	0.9089 0.9240 0.7226 0.7275	0.4120 0.4211 0.2597 0.2612	4.9572 4.9762 4.2874 4.3208	0.0040 0.0041 0.0023 0.0023	0.0826 0.0807 0.0668 0.0665	0.0124 0.0972 0.5074 0.5149	0.0800 2.6152 3.6259 3.5725
PD_V	$k_{p,m}$=1, $k_{d,m}$=1, $k_{SOC,m}$=1 $k_{p,m}$=1, $k_{d,M}$=200, $k_{SOC,m}$=1 $k_{p,M}$=200, $k_{d,m}$=1, $k_{SOC,m}$=1 $k_{p,M}$=200, $k_{d,M}$=200, $k_{SOC,m}$=1 $k_{p,m}$=1, $k_{d,m}$=1, $k_{SOC,M}$=200 $k_{p,m}$=1, $k_{d,M}$=200, $k_{SOC,M}$=200 $k_{p,M}$=200, $k_{d,m}$=1, $k_{SOC,M}$=200 $k_{p,M}$=200, $k_{d,M}$=200, $k_{SOC,M}$=200	Δk_p=10 Δk_d=10 Δk_{SOC}=10	0.0473 0.0481 0.0314 0.0318 0.0475 0.0481 0.0475 0.0482	0.9083 0.9242 0.7250 0.7284 0.9137 1.0367 0.7923 0.8102	0.4119 0.4214 0.2603 0.2620 0.4132 0.4473 0.4062 0.4152	4.9578 4.9831 4.2910 4.3303 5.0017 5.8929 4.5434 4.5442	0.0040 0.0041 0.0023 0.0023 0.0040 0.0042 0.0036 0.0038	0.0826 0.0808 0.0671 0.0667 0.0828 0.0874 0.0732 0.0753	0.0082 0.0953 0.4925 0.5006 0.0010 0.0645 0.1693 0.1817	0.0775 2.5883 3.6146 3.5616 0.0387 2.3586 3.3140 3.3255
NLP	vtx_m=0.1 vtx_M=1.5	Δvtx=0.02	0.0215 0.0246	0.6770 0.8445	0.2307 0.3327	4.3514 4.6110	0.0146 0.0060	0.0703 0.0772	3.9519 1.2201	3.9794 1.3237
NLP_V	$vtx_{max,m}$=1, $f_{band,m}$=0.5 $vtx_{max,m}$=1, $f_{band,M}$=2 $vtx_{max,M}$=1.5, $f_{band,m}$=0.5 $vtx_{max,M}$=1.5, $f_{band,M}$=2	Δvtx_{max}=0.02 Δf_{band}=0.05	0.0191 0.0209 0.0220 0.0240	0.7194 0.7505 0.7253 0.7873	0.2198 0.2677 0.2697 0.3159	4.2824 4.2124 4.2338 4.1509	0.0085 0.0087 0.0057 0.0060	0.0676 0.0720 0.0680 0.0751	1.8848 1.8030 1.3026 1.2380	3.6905 3.0955 3.4936 2.3533

REFERENCES

[1] REN21. (2020). *Renewables 2020 Global Status Report*. [Online]. Available: https://www.ren21.net/reports/global-status-report/

[2] European Council. (2014). *Conclusions EUCO 169/14*. Brussels, Belgium. [Online]. Available: http://data.consilium.europa.eu/doc/document/ST-169-2014-INIT/en/pdf

[3] *Energy Roadmap 2050*, European Council, Brussels, Belgium, 2012, doi: 10.2833/10759.

[4] G. E. Halkos and E.-C. Gkampoura, "Reviewing usage, potentials, and limitations of renewable energy sources," *Energies*, vol. 13, no. 11, p. 2906, Jun. 2020, doi: 10.3390/en13112906.

[5] R. Karki and R. Billinton, "Reliability/cost implications of PV and wind energy utilization in small isolated power systems," *IEEE Trans. Energy Convers.*, vol. 16, no. 4, pp. 368–373, Dec. 2001, doi: 10.1109/60.969477.

[6] G. Caralis and A. Zervos, "Analysis of the combined use of wind and pumped storage systems in autonomous Greek islands," *IET Renew. Power Generation*, vol. 1, no. 1, pp. 49–60, Mar. 2007, doi: 10.1049/iet-rpg:20060010.

[7] D. M. Gioutsos, K. Blok, L. van Velzen, and S. Moorman, "Cost-optimal electricity systems with increasing renewable energy penetration for islands across the globe," *Appl. Energy*, vol. 226, pp. 437–449, Sep. 2018, doi: 10.1016/j.apenergy.2018.05.108.

[8] M. H. Albadi and E. F. El-Saadany, "Overview of wind power intermittency impacts on power systems," *Elect. Power Syst. Res.*, vol. 80, no. 6, pp. 627–632, Jun. 2010, doi: 10.1016/j.epsr.2009.10.035.

[9] P. S. Georgilakis, "Technical challenges associated with the integration of wind power into power systems," *Renew. Sustain. Energy Rev.*, vol. 12, no. 3, pp. 852–863, 2008, doi: 10.1016/j.rser.2006.10.007.

[10] R. S. Kaneshiro, "Hawaii island (big island) wind impact," in *Proc. Workshop Active Power Control From Wind Power*, Broomfield, CO, USA, vol. 17, May 2013.

[11] S. Sharma, S.-H. Huang, and N. D. R. Sarma, "System inertial frequency response estimation and impact of renewable resources in ERCOT interconnection," in *Proc. IEEE Power Energy Soc. Gen. Meeting*, Jul. 2011, pp. 1–6, doi: 10.1109/PES.2011.6038993.

[12] Y. Wang, V. Silva, and M. Lopez-Botet-Zulueta, "Impact of high penetration of variable renewable generation on frequency dynamics in the continental Europe interconnected system," *IET Renew. Power Gener.*, vol. 10, no. 1, pp. 10–16, Jan. 2016, doi: 10.1049/iet-rpg.2015.0141.

[13] H. R. Iswadi, R. J. Best, and D. J. Morrow, "Irish power system primary frequency response metrics during different system non synchronous penetration," in *Proc. IEEE Eindhoven PowerTech*, Jun. 2015, pp. 1–6, doi: 10.1109/PTC.2015.7232425.

[14] L. Sigrist, L. Rouco, and F. M. Echavarren, "A review of the state of the art of UFLS schemes for isolated power systems," *Int. J. Elect. Power Energy Syst.*, vol. 99, pp. 525–539, Jul. 2018, doi: 10.1016/j.ijepes.2018.01.052.

[15] N. Hamsic, A. Schmelter, A. Mohd, E. Ortjohann, E. Schultze, A. Tuckey, and J. Zimmermann, "Increasing renewable energy penetration in isolated grids using a flywheel energy storage system," in *Proc. Int. Conf. Power Eng., Energy Electr. Drives*, Apr. 2007, pp. 195–200, doi: 10.1109/POWERENG.2007.4380112.

[16] G. Delille, B. Francois, and G. Malarange, "Dynamic frequency control support by energy storage to reduce the impact of wind and solar generation on isolated power system's inertia," *IEEE Trans. Sustain. Energy*, vol. 3, no. 4, pp. 931–939, Oct. 2012, doi: 10.1109/TSTE.2012.2205025.

[17] L. Kane and G. Ault, "A review and analysis of renewable energy curtailment schemes and principles of access: Transitioning towards business as usual," *Energy Policy*, vol. 72, pp. 67–77, Sep. 2014, doi: 10.1016/j.enpol.2014.04.010.

[18] Y. Li, S. S. Choi, D. M. Vilathgamuwa, B. Xiong, and J. Tang, "Combined primary frequency and virtual inertia response control scheme of a variable-speed dish-stirling system," *IEEE Access*, vol. 8, pp. 151719–151730, 2020, doi: 10.1109/ACCESS.2020.3017791.

[19] K. Singh, "Enhancement of frequency regulation in tidal turbine power plant using virtual inertia from capacitive energy storage system," *J. Energy Storage*, vol. 35, Mar. 2021, Art. no. 102332, doi: 10.1016/j.est.2021.102332.

[20] A. Aziz, A. Than Oo, and A. Stojcevski, "Frequency regulation capabilities in wind power plant," *Sustain. Energy Technol. Assessments*, vol. 26, pp. 47–76, Apr. 2018, doi: 10.1016/j.seta.2017.10.002.

[21] H. Badihi, Y. Zhang, and H. Hong, "Active power control design for supporting grid frequency regulation in wind farms," *Annu. Rev. Control*, vol. 40, pp. 70–81, Jan. 2015, doi: 10.1016/j.arcontrol.2015.09.005.

[22] G. Lalor, A. Mullane, and M. O'Malley, "Frequency control and wind turbine technologies," *IEEE Trans. Power Syst.*, vol. 20, no. 4, pp. 1905–1913, Nov. 2005, doi: 10.1109/TPWRS.2005.857393.

[23] J. Morren, S. W. H. de Haan, W. L. Kling, and J. A. Ferreira, "Wind turbines emulating inertia and supporting primary frequency control," *IEEE Trans. Power Syst.*, vol. 21, no. 1, pp. 433–434, Feb. 2006, doi: 10.1109/TPWRS.2005.861956.
[24] A. Mullane and M. O'Malley, "The inertial response of induction-machine-based wind turbines," *IEEE Trans. Power Syst.*, vol. 20, no. 3, pp. 1496–1503, Aug. 2005, doi: 10.1109/TPWRS.2005.852081.
[25] G. Martínez-Lucas, J. I. Sarasúa, J. I. Pérez-Díaz, S. Martínez, and D. Ochoa, "Analysis of the implementation of the primary and/or inertial frequency control in variable speed wind turbines in an isolated power system with high renewable penetration. Case study: El Hierro power system," *Electronics*, vol. 9, no. 6, p. 901, May 2020, doi: 10.3390/electronics9060901.
[26] Z. Ding, F. Teng, P. Sarikprueck, and Z. Hu, "Technical review on advanced approaches for electric vehicle charging demand management, Part II: Applications in transportation system coordination and infrastructure planning," *IEEE Trans. Ind. Appl.*, vol. 56, no. 5, pp. 5695–5703, Sep. 2020, doi: 10.1109/TIA.2020.2993760.
[27] P. Jampeethong and S. Khomfoi, "Coordinated control of electric vehicles and renewable energy sources for frequency regulation in microgrids," *IEEE Access*, vol. 8, pp. 141967–141976, 2020, doi: 10.1109/ACCESS.2020.3010276.
[28] P. Meibom, R. Barth, B. Hasche, H. Brand, C. Weber, and M. O'Malley, "Stochastic optimization model to study the operational impacts of high wind penetrations in Ireland," *IEEE Trans. Power Syst.*, vol. 26, no. 3, pp. 1367–1379, Aug. 2011, doi: 10.1109/TPWRS.2010.2070848.
[29] A. Tascikaraoglu and M. Uzunoglu, "A review of combined approaches for prediction of short-term wind speed and power," *Renew. Sustain. Energy Rev.*, vol. 34, pp. 243–254, Jun. 2014, doi: 10.1016/j.rser.2014.03.033.
[30] G. Papaefthymiou and K. Dragoon, "Towards 100% renewable energy systems: Uncapping power system flexibility," *Energy Policy*, vol. 92, pp. 69–82, May 2016, doi: 10.1016/j.enpol.2016.01.025.
[31] M. Valavi and A. Nysveen, "Variable-speed operation of hydropower plants: A look at the past, present, and future," *IEEE Ind. Appl. Mag.*, vol. 24, no. 5, pp. 18–27, Sep./Oct. 2018.
[32] R. Raja Singh, T. Raj Chelliah, and P. Agarwal, "Power electronics in hydro electric energy systems—A review," *Renew. Sustain. Energy Rev.*, vol. 32, pp. 944–959, Apr. 2014, doi: 10.1016/j.rser.2014.01.041.
[33] J. I. Sarasúa, G. Martínez-Lucas, C. A. Platero, and J. Sánchez-Fernández, "Dual frequency regulation in pumping mode in a wind–hydro isolated system," *Energies*, vol. 11, no. 11, p. 2865, 2018, doi: 10.3390/en11112865.
[34] X. Luo, J. Wang, M. Dooner, and J. Clarke, "Overview of current development in electrical energy storage technologies and the application potential in power system operation," *Appl. Energy*, vol. 137, pp. 511–536, Jan. 2015, doi: 10.1016/j.apenergy.2014.09.081.
[35] T.-T. Nguyen, V. Martin, A. Malmquist, and C. A. S. Silva, "A review on technology maturity of small scale energy storage technologies," *Renew. Energy Environ. Sustainability*, vol. 2, p. 36, Jan. 2017, doi: 10.1051/rees/2017039.
[36] N. W. Miller, M. Shao, S. Pajic, and R. D'Aquila, "Western wind and solar integration study phase 3–frequency response and transient stability," Nat. Renew. Energy Lab., Golden, CO, USA, GE Energy Manage., Schenectady, NY, USA, Tech. Rep. NREL/SR-5D00-62906, 2014.
[37] L. Meng, J. Zafar, S. K. Khadem, and A. Collins, "Fast frequency response from energy storage systems—A review of grid standards, projects and technical issues," *IEEE Trans. Smart Grid*, vol. 11, no. 2, pp. 1566–1581, Mar. 2020, doi: 10.1109/TSG.2019.2940173.
[38] M. Szablicki, P. Rzepka, P. Sowa, and A. Halinka, "Energy storages as synthetic inertia source in power systems," in *Proc. IEEE 38th Central Amer. Panama Conv. (CONCAPAN XXXVIII)*, Nov. 2018, pp. 1–6, doi: 10.1109/CONCAPAN.2018.8596425.
[39] F. Goris and E. L. Severson, "A review of flywheel energy storage systems for grid application," in *Proc. 44th Annu. Conf. IEEE Ind. Electron. Soc. (IECON)*, Oct. 2018, pp. 1633–1639, doi: 10.1109/IECON.2018.8591842.
[40] T. Engelmann, R. vor dem Esche, and R. Tudi, "Fast response flywheel energy storage technology for virtual power plants and microgrids," in *Proc. Elect. Energy Storage Appl. Technol.*, 2017, pp. 1–11.
[41] X. Li and A. Palazzolo, "A review of flywheel energy storage systems: State of the art and opportunities," *J. Energy Storage*, vol. 46, Feb. 2022, Art. no. 103576, doi: 10.1016/j.est.2021.103576.
[42] M. E. Amiryar and K. R. Pullen, "A review of flywheel energy storage system technologies and their applications," *Appl. Sci.*, vol. 7, no. 3, p. 286, 2017, doi: 10.3390/app7030286.
[43] M. L. Lazarewicz and T. M. Ryan, "Integration of flywheel-based energy storage for frequency regulation in deregulated markets," in *Proc. IEEE PES Gen. Meeting*, Jul. 2010, pp. 4–9, doi: 10.1109/PES.2010.5589748.
[44] H. Vasconcelos, C. Moreira, A. Madureira, J. P. Lopes, and V. Miranda, "Advanced control solutions for operating isolated power systems: Examining the Portuguese islands," *IEEE Electrific. Mag.*, vol. 3, no. 1, pp. 25–35, 2015, doi: 10.1109/MELE.2014.2380131.
[45] S. Karrari, G. De Carne, and M. Noe, "Model validation of a high-speed flywheel energy storage system using power hardware-in-the-loop testing," *J. Energy Storage*, vol. 43, Nov. 2021, Art. no. 103177, doi: 10.1016/j.est.2021.103177.
[46] S. S. Sami, M. Cheng, and J. Wu, "Modelling and control of multi-type grid-scale energy storage for power system frequency response," in *Proc. IEEE 8th Int. Power Electron. Motion Control Conf. (IPEMC-ECCE Asia)*, May 2016, pp. 269–273, doi: 10.1109/IPEMC.2016.7512297.
[47] S. Saberi Oskouee, S. Kamali, and T. Amraee, "Primary frequency support in unit commitment using a multi-area frequency model with flywheel energy storage," *IEEE Trans. Power Syst.*, vol. 36, no. 6, pp. 5105–5119, Nov. 2021, doi: 10.1109/TPWRS.2021.3074634.
[48] R. Sebastián and R. Peña-Alzola, "Control and simulation of a flywheel energy storage for a wind diesel power system," *Int. J. Electr. Power Energy Syst.*, vol. 64, pp. 1049–1056, Jan. 2015, doi: 10.1016/j.ijepes.2014.08.017.
[49] R. Takahashi and J. Tamura, "Frequency stabilization of small power system with wind farm by using flywheel energy storage system," in *Proc. IEEE Int. Symp. Diag. Electr. Mach., Power Electron. Drives*, Sep. 2007, pp. 393–398, doi: 10.1109/DEMPED.2007.4393126.
[50] I. Sarasúa, B. Torres, J. I. Pérez-Díaz, and M. Lafoz, "Control strategy and sizing of a flywheel energy storage plant for the frequency control of an isolated power system," in *Proc. 15th Wind Integr. Workshop*, 2016, pp. 1–7.
[51] A. M. Quevedo, R. C. de León, and J. G. Moreno, "Gorona del Viento wind-hydro power plant," in *Proc. 3rd Int. Hybrid Power Syst. Work.*, May 2018, pp. 1–9.
[52] J. O'Sullivan, A. Rogers, D. Flynn, P. Smith, A. Mullane, and M. O'Malley, "Studying the maximum instantaneous non-synchronous generation in an island system—Frequency stability challenges in Ireland," *IEEE Trans. Power Syst.*, vol. 29, no. 6, pp. 2943–2951, Nov. 2014, doi: 10.1109/TPWRS.2014.2316974.
[53] M. R. Rapizza and S. M. Canevese, "Fast frequency regulation and synthetic inertia in a power system with high penetration of renewable energy sources: Optimal design of the required quantities," *Sustain. Energy, Grids Netw.*, vol. 24, Dec. 2020, Art. no. 100407, doi: 10.1016/j.segan.2020.100407.
[54] K. Liu, J. He, Z. Luo, X. Shen, X. Liu, and T. Lu, "Secondary frequency control of isolated microgrid based on LADRC," *IEEE Access*, vol. 7, pp. 53454–53462, 2019, doi: 10.1109/ACCESS.2019.2911911.
[55] G. Martínez-Lucas, J. I. Sarasúa, J. Sánchez-Fernández, and J. R. Wilhelmi, "Power-frequency control of hydropower plants with long penstocks in isolated systems with wind generation," *Renew. Energy*, vol. 83, pp. 245–255, Nov. 2015, doi: 10.1016/j.renene.2015.04.032.
[56] A. Fernández-Guillamón, J. I. Sarasúa, M. Chazarra, A. Vigueras-Rodríguez, D. Fernández-Muñoz, and Á. Molina-García, "Frequency control analysis based on unit commitment schemes with high wind power integration: A Spanish isolated power system case study," *Int. J. Electr. Power Energy Syst.*, vol. 121, Oct. 2020, Art. no. 106044, doi: 10.1016/j.ijepes.2020.106044.
[57] CD Llanos Blancos. (2018). *Declaración Ambiental Enero-Diciembre*. [Online]. Available: https://www.endesa.com/
[58] J. I. Sarasúa, G. Martínez-Lucas, and M. Lafoz, "Analysis of alternative frequency control schemes for increasing renewable energy penetration in El Hierro island power system," *Int. J. Electr. Power Energy Syst.*, vol. 113, pp. 807–823, Dec. 2019, doi: 10.1016/j.ijepes.2019.06.008.
[59] J. Torres, P. Moreno–Torres, G. Navarro, M. Blanco, and M. Lafoz, "Fast energy storage systems comparison in terms of energy efficiency for a specific application," *IEEE Access*, vol. 6, pp. 40656–40672, 2018, doi: 10.1109/ACCESS.2018.2854915.
[60] *Red Electrica de España. El Hierro—Seguimiento de la Demanda de Energía Eléctrica*. Accessed: Nov. 4, 2021. [Online]. Available: https://demanda.ree.es/visiona/canarias/el_hierro/total
[61] M. A. Tankari, M. B. Camara, B. Dakyo, and G. Lefebvre, "Use of ultracapacitors and batteries for efficient energy management in wind–diesel hybrid system," *IEEE Trans. Sustain. Energy*, vol. 4, no. 2, pp. 414–424, Apr. 2013, doi: 10.1109/TSTE.2012.2227067.

[62] W. Yang, P. Norrlund, L. Saarinen, J. Yang, W. Guo, and W. Zeng, "Wear and tear on hydro power turbines–influence from primary frequency control," *Renew. Energy*, vol. 87, pp. 88–95, Mar. 2016, doi: 10.1016/j.renene.2015.10.009.
[63] W. Yang, P. Norrlund, and J. Yang, "Analysis on regulation strategies for extending service life of hydropower turbines," in *Proc. IOP Conf., Earth Environ. Sci.*, 2016, vol. 49, no. 5, Art. no. 052013, doi: 10.1088/1755-1315/49/5/052013.
[64] Alaska Center for Energy and Power (ACEP). (2019). *Composite Flywheels for Energy Storage*. [Online]. Available: https://acep.uaf.edu/
[65] VYCON. *REGEN Energy Recycling System*. Accessed: Nov. 5, 2021. [Online]. Available: https://vyconenergy.com/products/

HILEL GARCÍA-PEREIRA was born in Madrid, Spain, in 1994. He received the B.S. and M.S. degrees in industrial engineering from the Technical University of Madrid, Spain, in 2018 and 2020, respectively, where he is currently pursuing the Ph.D. degree in civil engineering.

Since 2020, he has been a Researcher with the Department of Hydraulic, Energy, and Environmental Engineering, Technical University of Madrid. His research interests include fast energy storage systems, frequency control involving renewable energy, and electrical drive control.

MARCOS BLANCO was born in Madrid, Spain, in 1983. He received the M.S. degree in industrial engineering and the Ph.D. degree in electrical engineering from the Technical University of Madrid, Spain, in 2008 and 2016, respectively.

He is currently a Researcher at the Electric Engineering Division of the CIEMAT, a Spanish Public Research Center. He is the coauthor of more than 20 journal articles and six patents. His expertise is focused on electrical drives control, power electronic converters, DSP-based control, and optimization algorithms. His main research interests include ocean wave energy generation, grid integration of renewable energy, and energy storage systems.

GUILLERMO MARTÍNEZ-LUCAS was born in Madrid, Spain, in 1989. He received the B.S., M.S., and Ph.D. degrees in civil engineering from the Technical University of Madrid, Spain, in 2013 and 2018, respectively.

Since 2016, he has been an Assistant Professor with the Department of Hydraulic, Energy and Environmental Engineering, Technical University of Madrid. He has participated in seven projects and research projects, with both public and private economic support and from national and international institutions, and is the author/coauthor of 15 journal articles included in the journal citations reports (JCR). His research interests include frequency control of isolated power systems with high renewable energy penetration.

JUAN I. PÉREZ-DÍAZ received the Ph.D. degree from the Technical University of Madrid (UPM), in 2008. He worked as an Assistant Professor with the UPM, until 2009, as a Non-Tenured Associate Professor, until 2020, and as an Associate Professor, since 2020. His current research interests include the application of optimization methods to the generation scheduling of electricity generation and storage systems and on the analysis of the system's frequency control under high penetration of renewable generation and energy storage.

JOSÉ-IGNACIO SARASÚA received the master's degree in civil engineering and the Ph.D. degree in civil engineering: hydraulic and energy from the Technical University of Madrid, in 2001 and 2009, respectively.

From 2002 to 2011, he worked as an Assistant Professor at Alfonso X University, and collaborated with several companies related to environmental issues. Since 2011, he has been an Assistant Professor at the Technical University of Madrid. He is the author of more than 20 articles. His research interests include the study of the impact of renewable energy penetration, especially in isolated power systems, the frequency control developed by hydroelectric groups, and fast energy storage systems, such as flywheels plants, and coordinated control actions involving renewable energy sources, such as wind turbines, PV plants, and hydroelectric units.